Small

NANO · MICRO small
www.small-journal.com

PERSPECTIVE OPEN ACCESS

Sodium-Based Battery Component Design: Imitating Lithium or Forging New Paths?

Xingxing Wang[1] | Ziyu Song[1] | Wenfang Feng[1] | Moritz Schütte[2] | Sascha Berg[2,3] | Feng Cai[2] | Viviane Maccio-Figgemeier[2,3] | Dirk Uwe Sauer[2,3] | Stefano Passerini[4,5] | Michel Armand[6] | Zhibin Zhou[1] | Egbert Figgemeier[2,3] | Heng Zhang[1] | Gebrekidan Gebresilassie Eshetu[2,7]

[1]Key Laboratory of Material Chemistry for Energy Conversion and Storage (Ministry of Education), School of Chemistry and Chemical Engineering, Huazhong University of Science and Technology, Wuhan, China | [2]Institute of Power Electronics and Electric Drives (ISEA), Center for Ageing Reliability and Lifetime Prediction of Electrochemical and Power Electronic Systems (CARL), RWTH Aachen University, Aachen, Germany | [3]Helmholtz Institute Münster (HIMS), IMD-4, Forschungszentrum Jülich GmbH, Jülich, Germany | [4]International Electrochemical Energy Storage Research Institute (IEES), School of Energy and Mechanical Engineering, Nanjing Normal University, Nanjing, China | [5]Karlsruhe Institute of Technology (KIT) Helmholtz Institute Ulm (HIU), Ulm, Germany | [6]Centre for Cooperative Research on Alternative Energies (CIC energiGUNE), Basque Research and Technology Alliance (BRTA), Vitoria-Gasteiz, Spain | [7]Department of Material Science and Engineering, Mekelle Institute of Technology, Mekelle University, Mekelle, Ethiopia

Correspondence: Egbert Figgemeier (e.figgemeier@fz-juelich.de) | Heng Zhang (hengzhang2020@hust.edu.cn) | Gebrekidan Gebresilassie Eshetu (Gebrekidan.Eshetu@isea.rwth-aachen.de)

Received: 7 February 2026 | **Revised:** 10 April 2026 | **Accepted:** 21 May 2026

Keywords: cation chemistries | electrode materials | interfaces and interphases | lithium batteries | nonaqueous electrolytes | sodium batteries

ABSTRACT

Sodium-ion batteries (SIBs) are promising candidates for large-scale storage systems due to abundant Na resources, low costs, and a similar cell configuration to lithium-ion batteries (LIBs). However, due to the distinct physico-chemical properties of Li^+ and Na^+ cations, directly transferring concepts and established knowledge from LIBs to SIBs is unfeasible. Therefore, a new out-of-the-box perspective is required in the design of electrode materials, electrolytes, interphases, and other components to account for the unique characteristics of SIBs. This review clarifies the fundamental divergences between Li and Na from the viewpoint of their cation chemistry, including differences in atomic and ionic radii, electronegativity, polarizability and charge density. Based on the differences in cation chemistry, this review elaborates on their impacts on electrolyte bulk and interfacial properties, the design and selection of electrode materials, electrolytes, and the formation of interphases/interfaces. It highlights that the design of SIB components must be considered as independent systems with their own governing principles and design rules, rather than as direct derivatives of Li. This work offers critical insights for optimizing SIBs performance and advancing non-lithium mono-/multivalent cation batteries.

1 | Introduction

The massive demand for electric vehicles and the large-scale development and integration of renewable sustainable energies require cost-effective, high-energy-density, safer, and eco-friendly energy storage devices. Currently, the market is dominated by lithium-ion batteries (LIBs, Figure 1a) [1]. However, escalating concerns over the limited abundance, escalating geopolitical risk and rising cost of lithium (Li), reliance on critical and geopolitically sensitive minerals such as nickel (Ni) and cobalt (Co), and sustainability challenges create an urgent need to diversify contemporary battery chemistries [2, 3]. Sodium

Xingxing Wang and Ziyu Song contributed equally to this work.

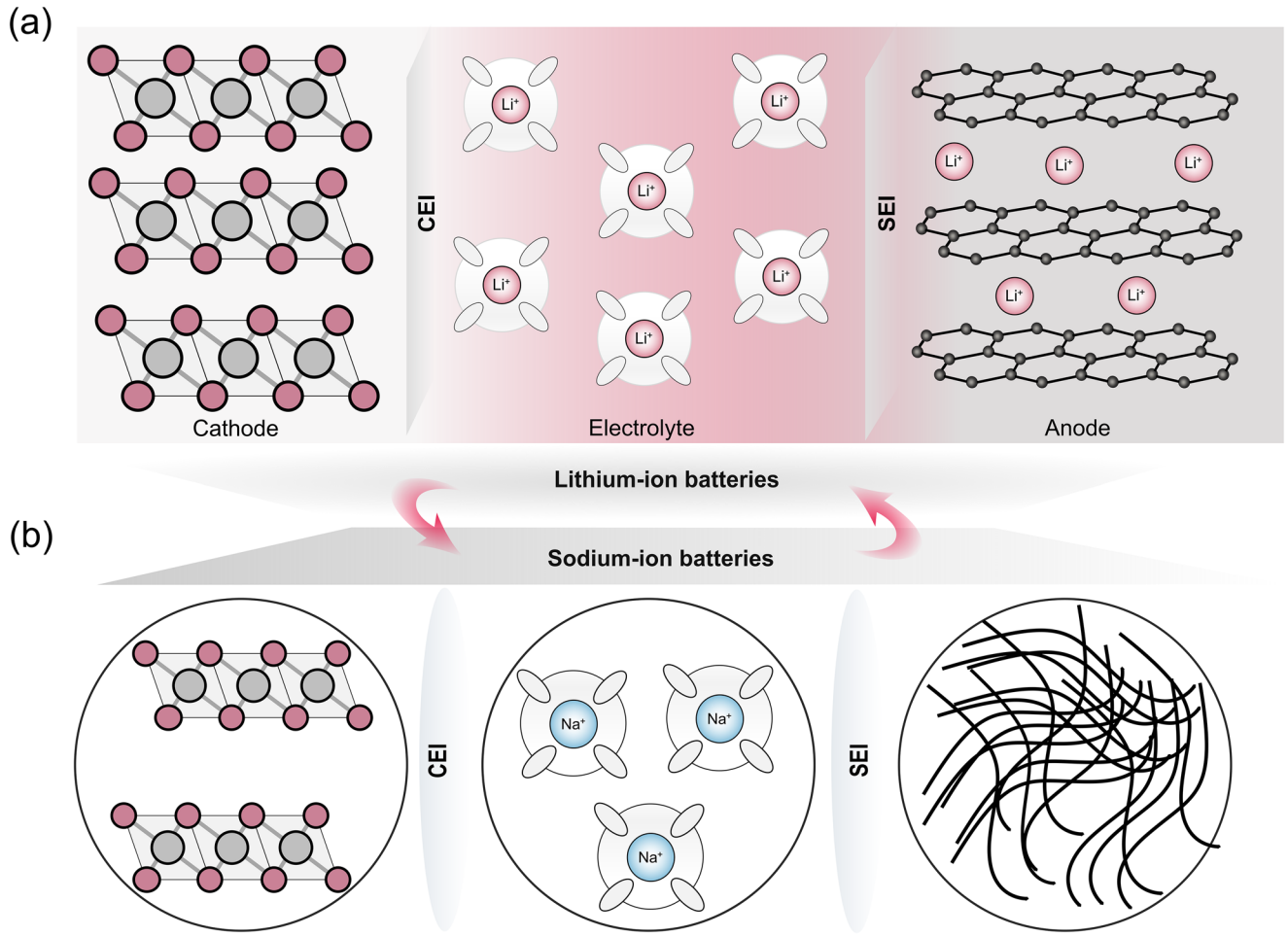

FIGURE 1 | Similarities and differences between Li- and Na-based rechargeable batteries. (a) General configuration and composition of LIBs, including cathode, anode, electrolyte, and Solid Electrolyte Interphase (SEI)/cathode Electrolyte Interphase (CEI) layers. (b) Re-examination of SIBs components, highlighting lessons learned from LIBs, and the need to rethink each element independently.

(Na)-based batteries have emerged as a promising complementary technology, leveraging abundant and low-cost materials, such as iron (Fe) and manganese (Mn) in cathodes, aluminium (Al) as negative electrode current collectors, and hard carbon (HC) as anode material, offering a safer and more sustainable path toward designing cheaper and environmentally benign battery systems [4–7]. It has to be emphasized that Li- and Na-based technologies are not rivals but serve distinct niche applications. Li is ideal for powering heavy-duty electric vehicles (EVs), as well as aerospace applications like drones, that demand high energy density and lightweight. In contrast, Na is well suited for light-duty vehicles, short-range mobility, grid and stationary energy storage, and industrial energy storage applications.

Sodium-ion batteries (SIBs) have advanced rapidly in recent years, in part because their energy storage mechanisms, cell components, and manufacturing processes closely resemble those of current LIBs [8–10]. R&D on Na-based batteries has grown substantially, frequently exploring materials analogous to those employed in Li-based batteries [7, 11–13]. However, the distinct chemistries of Li^+ and Na^+ cations introduce both challenges and opportunities in the design and selection of electrode materials, electrolytes, current collectors, and in the engineering of interphases and interfaces, safety, and other system-level factors, thereby requiring approaches that go beyond mere mimicry or copy-pasting.

SIBs are conceptually akin to LIBs but rely on Na^+ rather than Li^+ as mobile charge carrier cations. Thus, despite the valuable insights and lessons can be gained from Li-based systems, their direct translation to SIBs can remain unfeasible. Differences in operating voltage, Shannon radius, charge density, Pauling electronegativity, polarizing power, solvation energy, and other physico-chemical properties fundamentally impact the design and selection of electrode materials and reshape molecular-level interactions within the electrolyte bulk, which in turn govern the macroscopic electrolyte properties and the nature of the interfaces and interphases formed in the vicinity with the electrodes. Yet, the R&D trajectory of SIBs has largely followed the Li-ion tradition, often adopted fundamental principles wholesale and left a critical gap in the design, formulation, and understanding of electrodes, electrolytes, interphases, and safety appraisal in Na-based systems [14, 15]. Hence, there is an urgent need to reassess the design and understanding of electrodes, electrolytes, and interphases in SIBs through a new lens to unlock breakthrough advancements.

This Perspective goes beyond merely summarizing existing literature, aiming instead at redefining the approaches for selecting electrode active materials, designing electrolytes and interphases, and be comprehensive at safety validation for Na-based batteries. Traditional reviews often focus on incremental advances, but simply adapting LIBs principle is insufficient to achieve breakthroughs in both the fundamental understanding and large-scale deployment of SIBs. Building upon the preceding discussion, this Perspective explains why Na-based systems demand a fundamentally different conceptual and experimental framework, grounded in the unique physicochemical characteristics of Na. Specifically, this article (i) elucidates the key divergences between Li and Na from the perspective of their cation chemistry, (ii) highlights scientific blind spots that arise from reliance on Li^+ design principles through comparative meta-analyses, and (iii) proposes novel pathways to overcome these limitations by treating Na-based batteries as independent systems governed by their own principles, rather than as direct derivatives of Li (Figure 1b). Ultimately, this Perspective aims to emphasize the uniqueness of the Na^+ cation, highlight the chemical distinctions from Li-based systems, and inspire innovative research that accelerates the development of Na-based batteries as a robust and sustainable complement to Li-based technologies, and advancing end-to-end non-lithium mono- and multi-valent cation-based battery technologies.

2 | Fundamental Properties of Li vs. Na Cations and Their Implications

To understand the physico-chemical and electrochemical similarities and distinctions between Na^+ and Li^+ cation chemistries, several key thinking tools from a chemistry perspective can be adopted, including atomic and ionic volumes, Pauling electronegativity and bond polarizability, solvation energy, and redox potentials, etc. Below is a recap of how these thinking tools can be applied to the design of electrode materials, electrolytes, and interphases for Na-based systems, highlighting the limitations of directly transposing approaches developed for Li-based batteries.

2.1 | Atomic and Ionic Radii of Li vs. Na

In battery systems, the atomic and ionic radii of Li^+ and Na^+ are critical for understanding their spatial distribution and interactions not only within bulk electrolytes and electrode materials but also at the polarized electrode/electrolyte interfaces. Fundamentally, atomic and ionic radii are intrinsically linked to the electronic configurations of individual elements and their chemical interactions with neighboring species, with the radius offering precise insights into the local chemical environment of the element under investigation.

With the establishment of modern chemistry, the radius of an element is largely determined by the maximum charge density in its outermost orbitals [16]. However, defining an atomic radius in a physically rigorous way remains challenging, as it is a pragmatic conceptual tool rather than an intrinsic property of an element [17, 18]. The atomic radii of Na and Li reported in many textbooks are typically derived from their covalent radii in the condensed state (i.e., solid metals). The use of theoretical approaches based on quantum mechanics, however, enables relatively accurate estimations of atomic radius in the gas phases [19].

In the early 1920s, Lawrence Bragg derived the atomic radius of the sulfur atom by averaging the distances between two sulfur atoms in pyrite (FeS_2) crystals [20]. Subsequent crystallographic studies extended this approach, establishing empirical atomic radii for more than 40 elements, and accurately reproducing the bond lengths in a variety of ionic and metallic compounds, typically within a relatively high precision (0.06 Å) [20, 21]. Around the same time, Hüttig [22] investigated the ratios of anion to cation radii (i.e., ionic radius ratios) and their dependence on coordination environment, later linking these ratios concept to the packing efficiency of ionic crystals [23].

Intuitively, a clear distinction exists between atomic and ionic radii, as the monovalent Na^+ and Li^+ cations correspond to ionic species formed by removal of one electron from their respective elemental states Equation (1):

$$M \rightarrow M^+ + e^- \ (M = Na,\ Li) \tag{1}$$

Ionic radii are experimentally determined from crystallographic analyses of Na and Li metals and their ionic crystals, following the approach originally proposed by Bragg [20]. It is important to note that atoms in condensed matter cannot be treated perfectly as spherical nor rigid. Both the coordination environment and oxidation states have a significant impact on the radii of cations (and anions), with smaller radii observed for ions in higher oxidation states (i.e., stronger nuclear pull) or when coordinated by electron-donating ligands (e.g., F^-, $-C{\equiv}N$, $R_3P=O$, $C=O$) [19, 24]. For monovalent Na^+ and Li^+ cations, both the coordination number (CN) and cation occupancy significantly influence the ionic radii derived from crystallographic data. Table 1 provides a comparison of Li^+ and Na^+ radii, from various experimental and computational approaches.

In the 1970s, Shannon [24] revisited the experimental radii of a wide range of ions using crystallographic data and correlated these radius values with the corresponding oxidation states and coordination numbers. With a common CN of six, the ionic radii of Na^+ and Li^+ are 102 and 76 pm, respectively [24]. These values increase substantially when the coordinating ligands extend to eight (e.g., 116 pm vs. 102 pm for Na^+; 92 pm vs. 76 pm for Li^+). This clearly underscores the necessity of accounting for coordination environments when comparing and utilizing ionic radius data in battery research.

In addition to the ionic radii derived from crystallographic analyses, the van der Waals (VDW) radii, which reflect interatomic and intermolecular separation distances, provide valuable guidance for designing and optimizing electrolyte and electrode materials in Na- and Li-based batteries [29]. The simultaneous presence of electrostatic and van der Waals interactions in electrolyte solutions and electrode materials highlights the need for a reliable determination of the VDW radii of metal cations. In recent years, numerous theoretical approaches have been employed to determine the VDW radii [16], and a relatively consistent set of VDW radii for alkali metal cations has been reported in the recent computational work of Smith et al. [29]. As shown in Table 1, the VDW radii of both Na^+ and Li^+ cations are slightly larger than

TABLE 1 | Atomic and ionic radii of lithium and sodium.

Radius / pm	Li	Na	Refs.
Atom radius	152	186	[25]
Absolute atom radius	159	169	[26]
Shannon ionic radius	59 (IV) 76 (VI) 92 (VIII)	99 (IV) 100 (V) 102 (VI) 112 (VII) 116 (VIII) 124 (IX) 139 (XII)	[24]
Goldschmidt ionic radius	76	102	[27]
Pauling ionic radius	60	95	[28]
Wasastjerna ionic radius	68	101	[28]
VDW ionic radius	93	127	[29]
Absolute atom radius	19	32	[26]
Stokes solvated radius	480 (PC) 377 (MeOH) 292 (DMF) 298 (ACN) 192 (sulfolane)	460 (PC) 332 (MeOH) 246 (DMF) 310 (ACN) 230 (sulfolane)	[30]
NMR solvated radius	337 (71)	244 (97)	[31]

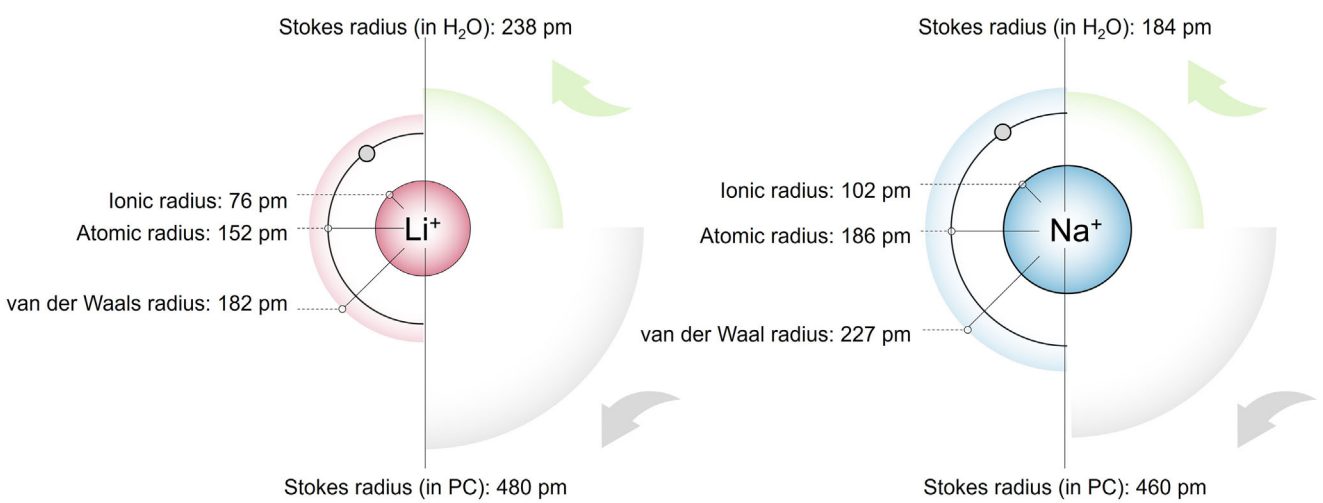

FIGURE 2 | Overview of Li^+ and Na^+ radii at different scales, including ionic, van der Waals, and Stokes radii.

the ionic radii (CN = 6) determined by Shannon, reflecting the combined influence of electrostatic and VDW interactions.

In solution chemistry, the effective ionic radii of both Na^+ and Li^+ cations increase due to solvation by solvent molecules (Figure 2). The correlation between ion diffusion and the radius of the solvated ion is described by the Stokes–Einstein equation Equation (2) [32–35]:

$$r = \frac{k_B T}{6\pi\eta D} \quad (2)$$

where k_B, T, η, and D denote the Boltzmann constant, temperature, viscosity, and ion diffusivity, respectively. Stokes ionic radii have been widely used to describe the solvation behavior of Na- and Li-based electrolytes [2]. As given in Table 1, the Stokes radius of Na^+ cation is slightly smaller than that of Li^+ cation in certain solvents [i.e., 460 pm (Na^+) vs. 480 pm (Li^+) in propylene carbonat (PC); 332 pm (Na^+) vs. 377 pm (Li^+) in methanol (MeOH)], though Na^+ occupies more space in ionic crystals. This behavior, however, is strongly related to the solvent identity, with the trend sometimes reversing when moving from protic to certain aprotic solvents (e.g., acetonitrile, sulfolane) [30].

The coefficient 6 in Equation 2 arises from the assumption of a perfect "stick" boundary condition, which assumes no relative tangential motion between the fluid and the sphere. If free tangential motion is allowed, this coefficient is reduced to 4. Hayamizu and co-workers employed [31] pulsed-field gradient nuclear magnetic resonance (PFG-NMR) to determine the Stokes ionic radii of various alkali metal ions in aqueous (water) solution. Based on their measurements, they proposed an intermediate state with a coefficient value of 4.8 for calculating the Stokes ionic radii, reflecting partial slip at the ion–water interface. Interestingly, a similar concept of an effective coefficient was introduced by Sounthland [36] in the early 1900s, predating the widely known Stokes–Einstein relation. As shown in Table 1, the Stokes ionic radii obtained from NMR are consistent with those derived from conductivity measurements in protic solvents [e.g., MeOH], and replacing Li with Na leads to a reduced hydration degree around the metal cations (Figure 2) [37, 38]. Such differences in the hydration degree between Li^+ and Na^+ cations can significantly influence the design of aqueous battery electrolytes, affecting both the degree of hydrogen evolution reaction (HER) and the oxygen evolution reaction (OER) [39, 40]. For the OER, the degree of hydration of ions could impact the OH^-/H_2O_2 to protons and O–O the dynamics of coupled steps, and it is reported that alkali metal cations (e.g., Li^+, Na^+) will change the its HER mechanism in the Pt electrode in alkaline medium [41].

Precisely identifying the boundary condition in the Stokes–Einstein expression is particularly important before directly applying Stokes ionic radii to the design of electrolytes and related battery materials [42]. For instance, large organic ions (e.g., ionic liquids) and concentrated electrolytes may deviate substantially from a perfect "sticky" boundary condition, introducing significant uncertainty in the determination of Stokes ionic radii.

2.2 | Electronegativity and Polarizability of Li vs. Na

Building on the discussion and conceptual insights of atomic and ionic radii, this section delves into examining the electronegativity and polarizability of metal cations, with a focus on the differences between Na- and Li-based systems. The electronegativity and polarizability of Li and Na are linked to their charge densities and Hard-Soft Acid-Base (HSAB) behavior. Generally, the small size of Li results in high charge density, higher electronegativity, and low polarizability, making it a hard acid. Na, being larger, has lower charge density and electronegativity but higher polarizability, making it relatively softer. Thus, size and charge density govern both their electron-attracting ability and acid-base character of the cations.

Electronegativity provides a quantitative measure of an atom's ability to attract electrons within a molecule. Pauling electronegativity is defined as the ability of an atom in a molecule to attract shared electrons toward itself [43, 44]. Extensive discussions of electronegativity and its applications can be found in standard chemistry textbooks and comprehensive reviews [45–47]. The inclusion of electronegativity in this context serves two purposes: 1) it helps in understanding the bonding interactions between atoms, provided a consistent electronegativity scale is used; and 2) modern electronegativity scales, which extend beyond Pauling's original concept, have been developed in recent years and may reform the design of nonaqueous electrolytes and advanced battery materials.

On the Pauling electronegativity scale, Na exhibits a slightly lower value than Li [i.e., 0.93 (Na) vs. 0.98 (Li), Table 2], a difference that is commonly adopted to rationalize the slightly stronger bond polarity of Li when paired with the same element. In contrast, the electronegativity values of Li and Na become comparable when using the scale proposed by Tandon et al. [48], while Na appears more electropositive than Li within the framework of the Allred–Rochow scale [49, 50] These discrepancies are closely related to the underlying methodologies of the respective electronegativity scales. In particular, the Pauling scale is derived from thermodynamic data of single covalent bonds, whereas alternative scales emphasize different physical descriptors, such as effective nuclear charge or electrostatic interactions.

In addition to electronegativity and polarizability, the ease with which the electron cloud of an ion can be distorted plays a critical role in dictating the electrolyte behavior. Li^+ cations, being smaller and more strongly attracted to electrons, exhibit lower polarizability, whereas Na^+ ions are larger, less electronegative, and more polarizable. These differences influence solvation structures, ion transport, and interfacial reactions in battery electrolytes, making a combined understanding of electronegativity and polarizability essential for rational electrolyte design and accompanying interfaces and interphases.

Polarizability is closely related to the change in electron density under an applied electric field, and characterizes the deformability of valence electrons. In general, polarizability scales are positively correlated with the size of an atom or ion [26]. Beyond the contribution of the outermost orbitals, recent density functional theory (DFT) studies suggest that the involvement of inner orbitals is also essential for accurately describing the polarizability of different atoms and ions [26]. In this context, Chen et al. [51]. comparatively investigated the chemical bonding of various sodium and lithium salts, and correlated the polarizability of Na^+ and Li^+ cations with their solubility in ionic liquids. By examining the distances between metal cation and anions, the authors observed significantly longer metal cation-anion separations for sodium salts compared to their lithium counterparts, sharing a common anion ($TFSI^-$, BF_4^- or PF_6^-), for example, 2.27–2.44 Å for Na salts vs. 1.86–1.98 Å for Li salts (Figure 3a). Orbital energy analyses revealed that the $2s^2$ electron in sodium cations are barely involved in bonding with the salt anions, whereas the $1s^2$ electrons of lithium cations actively participate in stabilizing the ion pairs, both in the gas phase and in solution (solvents). By correlating orbital energies with salt solubility, it becomes evident that the solubility of lithium salt increases with increasing bonding covalency (i.e., decreasing orbital energy), with TFSI and FSI-based salts exhibiting the highest solubility across various ionic liquids (Figure 3b,c). It should be noted that ionic liquids differ fundamentally from molecular solvents in terms of metal-ion solvation because of their distinct coordinating abilities per unit volume. Moreover, dissolution of metal salts in ionic liquids does not necessarily imply complete dissociation of ion pairs, which is typically required for efficient ion conduction in most liquid electrolytes. These insights indicate that a combined

TABLE 2 | Electronegativity of some alkali metals in different scales.[a]

Scaling method	Li	Na	K	Rb	Cs
Allred and Rochow	0.97	1.01	0.91	0.89	0.86
Pauling	0.98	0.93	0.82	0.82	0.79
Tandon et al.	1.00	1.00	0.93	0.92	0.91
Lang and Smith	1.24	1.18	1.00	0.96	0.89

[a]The values are adapted from ref. [49].

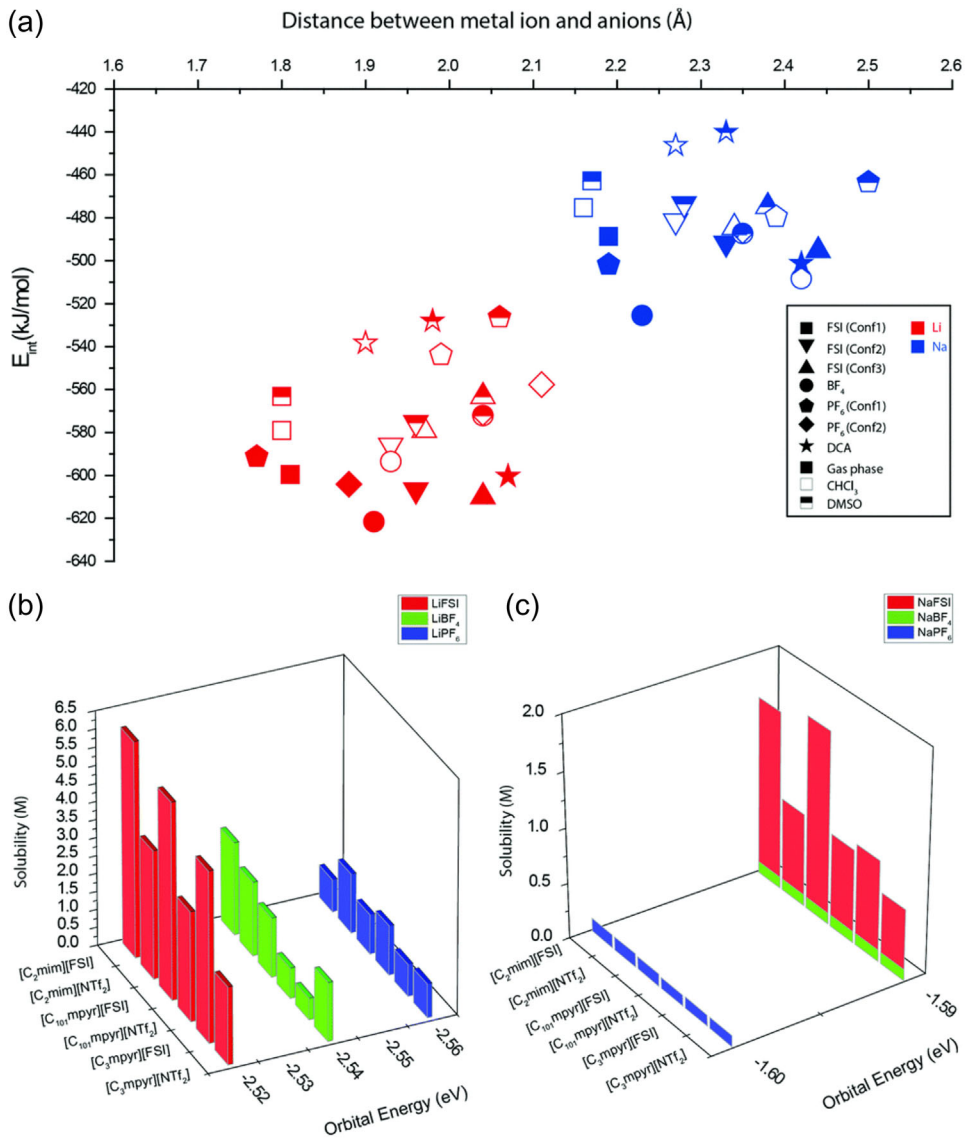

FIGURE 3 | (a) Inter-ionic distances (R, Å) and CCSD(T) full core interaction energies (EINT) of LiX and NaX (X = FSI, BF_4, PF_6, and DCA). (b,c) Solubility of MX in different ionic liquids: (b) LiX and (c) NaX (X = FSI, BF_4 and PF_6). Reproduced with permission [51]. Copyright 2017, The Royal Society of Chemistry.

understanding of cation polarizability, orbital participation, and solvation environment is critical for rationally designing battery electrolytes with optimized solubility and ionic transport properties, while also tailoring the composition, structure, and functionality of the interphases.

3 | Cation Chemistry–Guided Strategies for Electrode Design and Material Selection

Building upon the fundamental physico-chemical differences between Li^+ and Na^+ cations, this section examines the impact

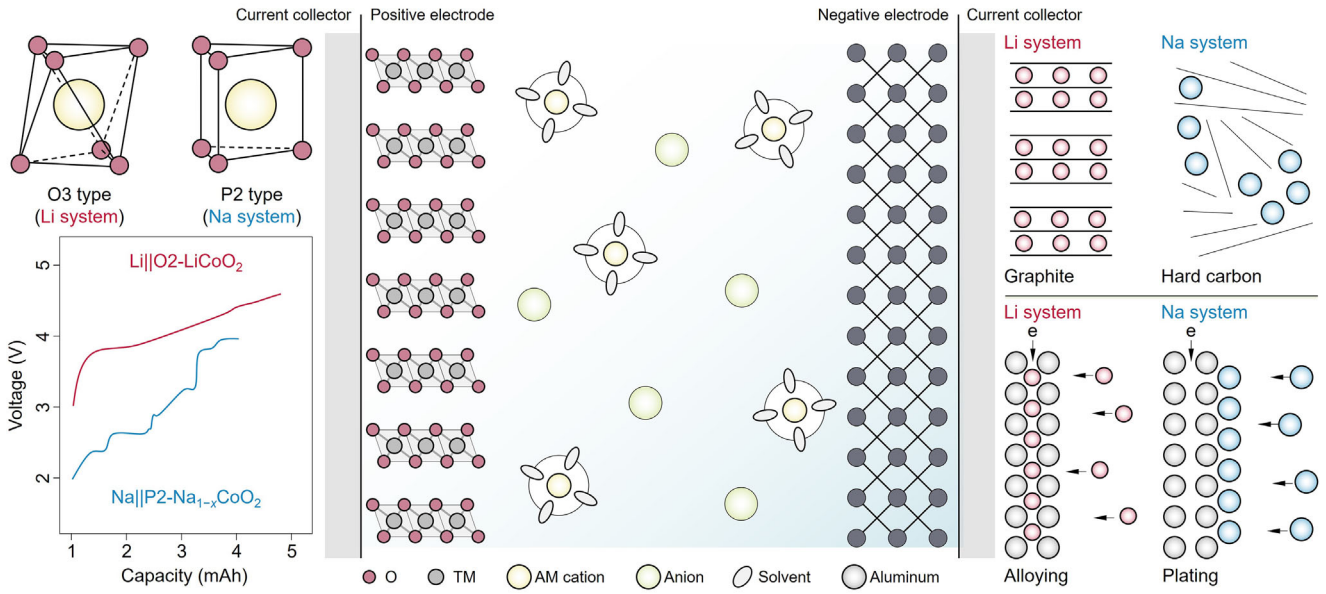

FIGURE 4 | Schematic diagram of the differences in the design principles of electrode systems for LIBs and SIBs.

of these differences on the design and selection of electrode materials.

3.1 | Impact of Cation Chemistry on Cathode Design and Selection

As discussed in the previous section, the chemistry and electrochemistry of electrode materials for SIBs differ significantly from those of their Li^+ counterparts. Materials that are compatible and perform well in Li-based systems may not be directly applicable to Na-based systems (Figure 4). This section succinctly explores how cation chemistry influences the design and selection of electrode materials. Layered oxides with the general formula $A_{1-x}MO_2$ (A = Li or Na, M = transition metal) consists of MO_2 slabs formed by edge-sharing MO_6 octahedra, with Li^+ or Na^+ cations occupying the interlayer spaces. These layered oxides can be classified as O2, O3, P2, or P3 types based on the stacking sequence of oxygen (O) along the c-axis, where 'O' indicates octahedral coordination of A^+ with oxygen, and P indicates coordination of A^+ with oxygen in a prismatic symmetry. Fuji's rule states that the preferred oxygen stacking type depends on the ratio of the A^+ cation to the transition metal cation radius, in that smaller A^+/M ratios favor octahedral coordination (O-type), whereas larger ratios stabilize prismatic coordination (P-type) [52–54]. This explains why Na^+, being larger than Li^+, commonly forms P2-type layered structures, while Li^+ favors O3-type stacking. Goldschmidt's tolerance factor (Equation 3) further predicts the geometric stability of the interlayer and framework structure, accounting for cation size mismatches and lattice distortions, which are particularly relevant for Na^+ insertion due to its larger ionic radius. Additionally, Pauling's rules regarding local charge balance and cation–anion coordination provide guidance on how A^+ ions distribute in the lattice and interact with the MO_2 framework. These combined descriptors, cation radius ratios, tolerance factors, and coordination preferences, allow prediction of structural stability, layer spacing, and diffusion pathways in layered oxides.

$$t = \frac{r_A + r_o}{\sqrt{2}(r_B + r_o)} \tag{3}$$

where t, r_A, r_B, and r_O denote the tolerance factor, A^+ cation radius, transition metal radius, and oxygen radius, respectively.

Goodenough et al. [55, 56]. report that stronger Co–O covalency in the Na system raises antibonding orbital energies, while increased Na^+–Na^+ repulsion elongates Co–O bonds at high Na^+ content, leading to lower voltages than in the Li system. Similarly, P2-type Na_xCoO_2 exhibits a lower voltage than O2-type $LiCoO_2$, owing to more covalent Co–O bonds, the weaker Lewis acidity of Na^+, and stronger Na^+–Na^+ repulsion compared to the corresponding Li^+ interactions. Moreover, depending on the A^+ ion, $LiCoO_2$ displays smooth galvanostatic charge–discharge curves, whereas Na_xCoO_2 shows an adjacent phases profile, regardless of its initial crystal structure (Figure 4). These typical cases highlight that the electrode's crystal structure determines how it interacts with different A^+ (Li^+ or Na^+) ions, meaning that a material suitable for Li^+ may not perform well with Na^+, and vice versa.

The chemistry of the intercalating cation also critically shapes the behavior of polyanion-type cathodes. Smaller cations like Li^+ fit easily into the rigid XO_4-based frameworks, enabling high voltages and fast diffusion, while larger cations such as Na^+ require more open lattices, which can reduce voltage, slow ion transport, and induce lattice strain. Optimizing the cation–polyanion match is therefore essential for achieving high energy density, good rate capability, and long-term structural stability [57].

3.2 | Impact of Cation Chemistry on Anode Design and Selection

From the perspective of the negative (anode) electrode, both LIBs and SIBs depend on carbonaceous materials for charge storage. However, the disparity in ionic radii between Li^+ and Na^+ critically influences which types of carbon structures are most suitable for efficient ion accommodation and reversible electrochemical performance. Graphite is the standard material for LIBs, largely because its layered structure enables reversible Li^+ intercalation with minimal structural strain [58, 59]. Graphene sheets in graphite are stacked via weak van der Waals forces with an interlayer spacing of ~3.35 Å, which is well-matched to the small size and strong interaction of Li^+ ions, allowing formation of stable graphite intercalation compounds such as LiC_6 with high reversible capacity of ~372 mAh g^{-1} and excellent cycle life. In contrast, conventional graphite does not serve as a suitable standard anode for SIBs under normal conditions. The larger Na^+ ions do not readily form stable binary graphite intercalation compounds because the graphite interlayer spacing is insufficient to accommodate Na^+ and the thermodynamics of Na–C bonding is unfavorable [5, 6]. First–principles studies show that the formation energy of Na–graphite intercalation compounds (NaC_x: NaC_6, NaC_8) is positive (thermodynamically unstable), in contrast to the favorable formation of Li–graphite compounds; this makes Na^+ insertion into graphite energetically unfavorable. In that case, the enthalpy penalty outweighs any entropy gain, resulting in $\Delta G > 0$ ($\Delta H \gg T\Delta S \Rightarrow \Delta G > 0$). For SIBs, hard carbon is the standard anode material because it can accommodate the larger Na^+ cations, which cannot intercalate efficiently into the tightly packed graphene layers. Hard carbon (HC) is a non-graphitizable, amorphous carbon consisting of disordered graphene sheets with irregular stacking, nanopores, and defects [60, 61]. The interlayer distances expand from ca. 3.3 Å to ca. 4.0 Å by replacing graphitic carbon with HC, resulting in weaker overlapping of the π-electrons among adjacent graphene layers [62]. During the electrochemical sodiation processes, the weak orbital hybridization with the reconstructed electron environment within in the disordered graphene layers provide electrostatic attraction to storage Na^+ ions. And the presence of hydrogen, heteroatoms, defective sites, and nanopores can increase the electron density of the local region, thus endowing HC materials with higher storage capability toward Na^+ ions [63–66]. Hence, the intercalations of Na^+ ions between slightly expanded graphene layers are generally accompanied by their adsorption at defect sites as well as nanopores filling processes, which jointly afford reversible capacities typically in the range of 250–350 mAh g^{-1}. Consequently, the disordered and porous structures empower the HC and related materials unique advantages as negative electrodes specifically for sodium batteries, rather than analogous lithium systems.

In general, the difference in ionic radii, charge density (ionic potential), and other physico-chemical between the two cations strongly influences the charge storage mechanisms. While lithium storage in graphite is dominated by intercalation, sodium storage in hard carbon involves not only limited intercalation but also significant contributions from adsorption at defect sites and pore filling, which play a decisive role in the overall capacity of hard carbon-based SIBs [67, 68]. From an electrochemical activity perspective, graphite in Li-based systems exhibits a well-defined voltage plateau at 0.1–0.2 V vs. Li/Li^+. In contrast, hard carbon in Na-based systems displays a combination of a sloping region and a low-voltage plateau (0.1–0.3 V vs. Na/Na^+), reflecting its more complex storage mechanisms [67, 68]. In the case of SIBs, the low-voltage plateau is primarily attributed to partial intercalation ($C_x + yNa^+ + ye^- \leftrightarrow Na_yC_x$) for the formation of sodium–graphite intercalation compounds (Na–GICs), whereas the sloping voltage region arises from Na^+ storage via nanopore filling and/or adsorption at defect sites ($C_{defect/pore} + Na^+ + e^- \leftrightarrow$ Na-$C_{adsorbed}$).

As noted above, it is well established that graphite exhibits negligible reversible Na^+ intercalation in conventional carbonate electrolytes (e.g., EC/DMC) at room temperature due to thermodynamic constraints. This limitation has motivated the widespread use of hard carbon and other non-graphitic carbons as anode materials in SIBs. In contrast, linear ethers, such as monoglyme, diglyme, and tetraglyme, enable the formation of Na^+–solvent complexes (e.g., Na^+–glyme) which enhance reversible capacity via a solvent co-intercalation mechanism, leading to the formation of so-called 'ternary graphite intercalation compounds' (tGICs) [69]. This process dynamically increases the interlayer spacing of graphite and stabilizes the inserted species. However, significant capacity loss is still observed during the initial cycles of graphite anodes in SIBs. This loss is generally attributed to irreversible electrolyte decomposition and the formation of SEI layers on the graphite surface. Despite these observations, the nature and local chemistry, thickness, and formation mechanism of this SEI layer remain poorly understood and continue to be a subject of debate. It has been reported using atomic force microscopy (AFM) that the Young's modulus of the surface of pristine graphite flakes (1.99 GPa) decreased significantly to 435.86 MPa after cycling, indicating the formation of a mechanically soft SEI layer on the graphite surface [70]. The local chemical composition of the SEI varies with the sodium salts and solvents used, and in ether-based electrolytes, it is typically thin (< 10 nm), comprising rigid inorganic components (NaF and Na_2CO_3) alongside flexible organic species (sodium alkoxides). In contrast, Goktas et al. [71] provided a fundamentally different perspective on SEI chemistry in graphite anodes for SIBs, suggesting that the byproducts of electrolyte decomposition are predominantly soluble or volatile, rather than forming a conventional solid SEI layer. This SEI-free perspective was further supported by Zhang et al., who reported that no SEI was observed on graphite flakes based on in situ AFM analysis [72]. These controversies underscore the urgent need for further in-depth investigation to elucidate both the existence and characteristics of SEI layers on graphite during co-intercalation reactions, thereby filling existing knowledge gaps and advancing understanding.

Alloy-type–based anodes represent another class of anode materials under exploration, where Li or Na is stored by forming intermetallic compounds, though their practical feasibility depends on both thermodynamics and kinetics. Li, being small and highly reactive, forms stable alloys with many metals and non-metals such as Si, Sn, Ge, and Al, because the Gibbs free energy of alloy formation is strongly negative (thermodynamically favorable) and Li diffuses quickly in host lattices (kinetically fast) [73]. Na, being larger and less reactive, can only alloy with heavier metals/metalloids like Sn, Sb, P, and Bi, as these structures can accommodate its size and provide negative Gibbs free energy.

Pure Si and Al, promising anode materials for LIBs, are not feasible for Na under normal conditions because their crystal lattices cannot accommodate the larger Na^+ ions, and the alloy formation is thermodynamically unfavorable ($\Delta G > 0$) [74]. However, by alloying with elements such as Sb, forming amorphous Sb-rich alloys or multilayer films, the thermodynamics and kinetics can be improved through structural reconstruction and the synergistic sodium storage effect, making Si an effective component of the anode in SIBs [75]. Kinetically, Na also diffuses more slowly, and its alloys undergo larger volume expansion, making cycling stability more challenging. In short, Li alloys are versatile due to favorable thermodynamics and fast kinetics, while Na alloys are limited to hosts that can structurally and energetically accommodate its larger size.

Regarding current collectors, copper (Cu) and aluminum (Al) are the most widely used materials for the anode and cathode, respectively, in LIBs. Cu is unsuitable as a cathode current collector because it undergoes oxidation at voltages above 3.38 V vs. Li/Li^+ [76, 77]. Conversely, Al cannot be used as an anode current collector for Li-based system, as it undergoes alloying with lithium at ca. 0.3 V vs. Li/Li^+ ($Al + xLi \leftrightarrow Li_xAl$), which is higher than that of the intercalation of Li^+ into graphite [78–80]. Unlike Li, Na does not electrochemically alloy with Al at room temperature (RT, 25°C) [81]. This allows the utilization of more cost-effective, light weight, cheaper, and abundant Al as the current collector to replace Cu at the anode side in SIBs. Such a substitution not only lowers the cost of SIBs but also enhances safety, as SIBs can be shipped fully discharged at 0 V, reducing transportation and storage risks [82].

In summary, the choice of cation, Li^+ or Na^+, critically affects the design and selection of both anode and cathode materials as well as current collectors. Despite belonging to the same group in the periodic table, their distinct properties lead to differences in voltage profiles, structural compatibility, and current collector requirements. These differences highlight that cation-specific interactions must guide electrode material design for optimal battery performance.

4 | Cation Chemistry–Directed Electrolyte Design and Formulation

This sub-section examines how cation chemistry fundamentally affects both the bulk and interfacial properties of electrolytes, highlighting why SIBs often require electrolyte optimization distinct from Li-based systems. At the outset, it must be clear that when a salt dissolves in a solvent, it forms a dynamic mixture with competing interactions between the various species, including cation–anion pairs, cation–solvent, anion–solvent, and solvent–solvent interactions, and free ions and solvent molecules. These molecular-level interactions, involving ionic bonds Equation (4), ion-dipole interactions Equation (5), hydrogen bonding, and dipole-dipole interactions Equation (6), are strongly influenced by the nature of the cations and their relative reactivity with the different components of the electrolyte (Figure 5) [83, 84].

$$U_{ion-ion=} - \frac{1}{4\pi\varepsilon} \times \frac{z_1 z_2 e^2}{r^2} \quad (4)$$

where $U_{\text{ion-ion}}$, ε, z_1, z_2, e, and r respectively correspond to the interactions between ions, the number of charges of two ions, the elementary charge, the dielectric constant of the solvent medium, and the distance between two ionic centers:

$$U_{ion-dipole=} - \frac{1}{4\pi\varepsilon} \times \frac{z_e \mu cos\theta}{r^2} \quad (5)$$

where $U_{\text{ion-dipole}}$, z_e, μ, and θ respectively correspond to the interactions between ions and polar molecules, the number of charges of the ion, the dipole moment of the polar molecules, and the Angle between the ion and the line connecting the positive and negative poles of the dipole:

$$U_{dipole-dipole=} - \frac{1}{(4\pi\varepsilon)^2} \times \frac{2\mu_1^2 \mu_2^2}{3k_B T r^6} \quad (6)$$

where $U_{\text{dipole-dipole}}$, μ_1, μ_2, k_B and T respectively correspond to the interactions between the polar molecules, the dipole moments of two polar molecules, the Boltzmann constant, and the thermodynamic temperature.

Such microscopic properties and interactions, in turn, significantly impact the electrolyte's macroscopic properties, including electrochemical stability, solvation dynamics, ion transport, and the formation and quality of interfaces and interphases, as well as safety. Collectively, these effects govern key performance metrics of the battery cell, including redox efficiency, rate capability, energy density, long-term cyclability, and safety.

4.1 | Solvation Parameters and Implications

In recent years, significant experimental and computational efforts have been devoted to gain atomic- and molecular- scale insight into the Na- and Li-based electrolytes [85, 86], and several solvent parameters have been suggested to accurately describe their solvation processes. Among these, the dielectric constant (ε) of a solvent, which quantifies its ability to separate charges, is a fundamental parameter in electrolyte design and dictating of the subsequent interfaces and interphases [84]. Organic cyclic carbonate solvents [e.g., ethylene carbonate (EC), and propylene carbonate (PC)] with high dielectric constant (> 65 at RT) are generally co-utilized with low ε organic linear carbonates such as dimethyl carbonate (DMC, $\varepsilon \sim 3$), diethyl carbonate (DEC, $\varepsilon \sim 2.8$) and ethyl-methyl carbonate (EMC, $\varepsilon \sim 2.9$) for formulating Na^+ and Li^+ conducting electrolytes [87]. High dielectric constant carbonates are particularly important for sodium electrolytes due to the generally lower solubility of sodium salts compared to lithium salts when paired with common salt anions (Figure 3, solubility in ionic liquids).

Another critical parameter is the electron-donating ability of the solvent, quantitatively characterized by the Gutmann donor number (DN, donicity, kcal mol^{-1}). This was originally determined by Gutmann et al. [88, 89] in the early 1960s, based on the enthalpy changes (ΔH) when a donating solvent (D) complexes with antimony (V) chloride ($SbCl_5$, Equation 7). The donor number, in synergy with the dielectric constant, can significantly accelerate the initial structural optimization of aprotic solvents. Solvents such as ethers, esters, amides, and others containing

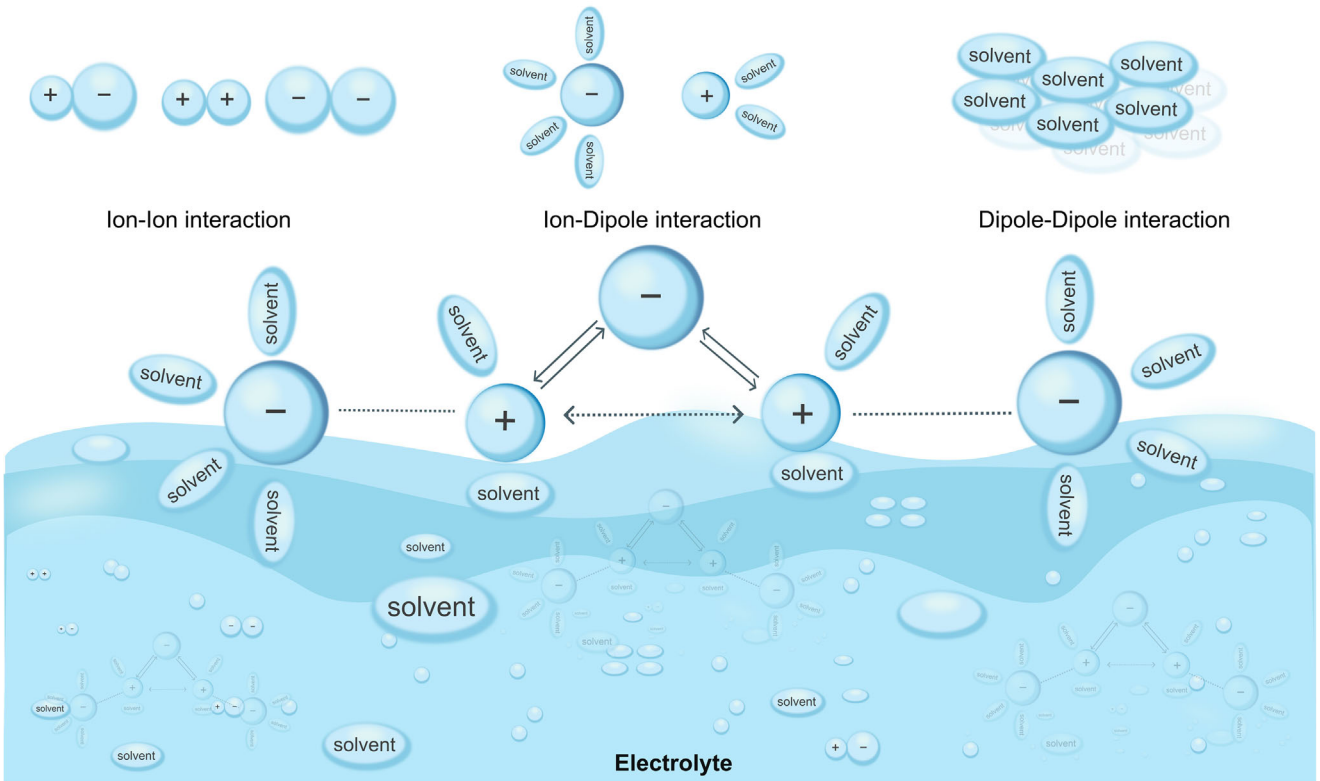

FIGURE 5 | Dissolution and dissociation of a metal (Li or Na) salt in dipolar aprotic solvent.

strong electron-donating groups are of particular interest for sodium electrolytes. Although the Gutmann donor number is a property of the solvent, the effective interaction of the solvent with the cation differs: Li^+, being smaller and more charge-dense, interacts more strongly with carbonate solvents than Na^+, resulting in a higher effective donor number for Li^+ and a correspondingly tighter solvation shell compared to the weaker solvation of Na^+.

$$D_{solvent}\,(dissolved) + SbCl_5\,(dissolved) \rightleftharpoons D \cdot SbCl_5\,(dissolved)$$

$$DN = -\Delta H_{D\Delta SbCl_5} \tag{7}$$

Of note, the selective interactions between solvent and metal salts are crucial for understanding the distinctions in the electrolyte chemistry of Na vs. Li. From the perspective of organic chemistry, ion pairing and its impact on the reactivity of metal alkoxides have been extensively investigated in the past decades [90]. The metal alkoxides exist in alcohol solution in many forms (Figure 6), enlisting solvent-separated ion pair (SSIP), solvent-shared ion pairs (SIP), and contact ion pairs (CIPs), as extensively reviewed by Msayib et al. [90] Most importantly, the formation and predominance of CIP, SIP, and SSIP are governed by the cation's size, charge density, and solvent dielectric constant. In that, small, highly charged cations (e.g., Li^+) favor CIPs in the solvents of low dielectric constant, large cations (K^+) favor solvent-separated ion pairs, and intermediate cations like sodium typically form SSIP or SIP at low concentrations, requiring higher concentrations or low-dielectric solvents to significantly populate CIPs. Such patterns in turn affect electrolyte bulk conductivity, viscosity, interfacial stability, and ultimately battery performance.

Figure 7a compares the association constant (K_{ass}) of alkoxide solutions consisting of alkali metal cations [90], and source data are available from the seminal work by Barthel et al. [91]. Longer alkyl chain length significantly increases the K_{ass} values for both Na- and Li-based systems, suggesting the decisive impact of dielectric properties of the parent alcohols. The correlation between K_{ass} values and cationic identity is not obvious, in which the reversed tendency occurs for Na vs. K when shifting from ethanol to propanol. Such a type of mismatch is also noticed by analyzing the degree of associations of these solutions (Figure 7b) [90]. It is thus critical to independently evaluate sodium, lithium, and potassium solutions by simultaneously diagnosing these cations with the employed solvents.

Host-guest chemistry provides a powerful framework for tuning solvent-salt interactions and ion-pairing equilibria in Na- and Li-based electrolytes. Alkali metal cation complexed with various molecular host materials have been extensively investigated in the past years [92–96], yielding thermodynamic parameters that are directly relevant to electrolyte design. Danil de Namor et al. [92]. reported the complexation thermodynamics of alkali metal cations with 5,11,17,23-tetra-tert-butyl [25,26,27,28-tetrakis(2-pyridylmethyl) oxy] calix(4)arene (Figure 7c), showing consistently higher values for Li-based complexes than for Na analogues as evidenced by larger log K_s values across aprotic solvents (Figure 7d). Such strong Li^+ coordination effectively competes with anion binding, shifting the ion-pairing equilibrium from contact and solvent-shared ion pairs toward

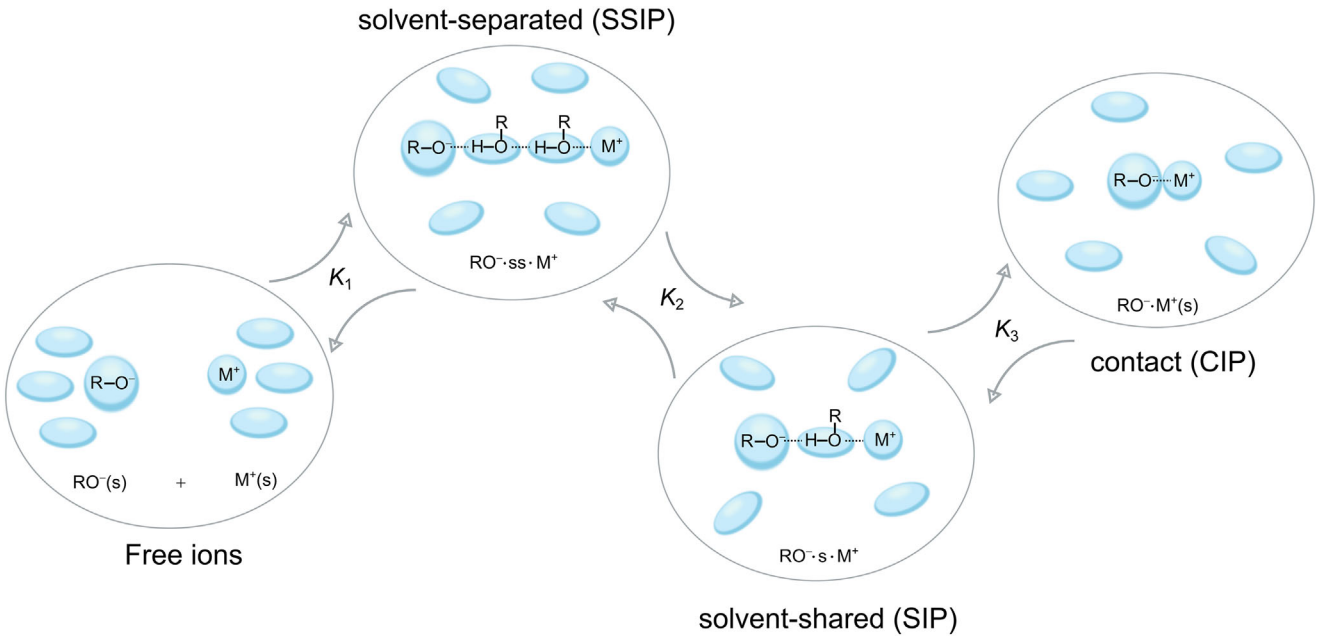

FIGURE 6 | Different ionic species in alkoxide solutions, including free ions, solvent-separated ion-pairs (SSIP), solvent-shared ion-pairs (SIP), and contact ion-pairs (CIP).

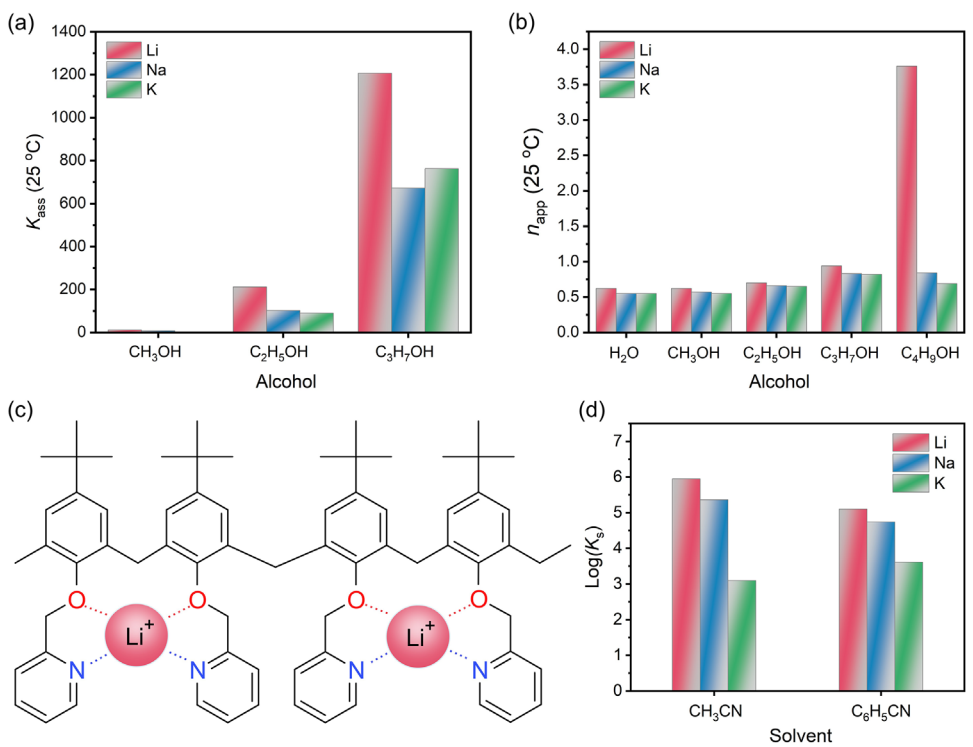

FIGURE 7 | (a,b) Association constant (K_{ass}) (a) and apparent degree of association (b) of alkali-metal cations in various alcohol solutions [90]. (c) Chemical structure of 5,11,17,23-tetra-tert-butyl [25,26,27,28-tetrakis(2-pyridylmethyl)oxy]calix(4)arene and its interaction with alkali-metal cations in ClO_4^- anion. (d) Stability constants (LogK_s) of different alkali-metal cations in acetonitrile and benzonitrile at RT [92].

solvent-separated ion pairs or free ions. Thus, compound 1a exhibits strong lithium selectivity (Figure 7c), however, this can be reversed by rational host-structure modification, as reviewed by Danil de Namor et al. [95]. Consequently, stability constants and Gibbs free energies of Li^+ and Na^+ complexes serve as quantitative descriptors for regulating CIP/SIP/SSIP populations, thereby controlling the bulk transport properties, interfacial chemistry, and ultimately battery performance.

4.2 | Cation-Dependent Solvation Structures in Electrolytes

Aforesaid distinct parameters determine the solvation structures of Li^+ and Na^+ in nonaqueous electrolytes. Due to its smaller ionic radius and higher charge density, Li^+ typically forms a more compact and strongly bound solvation shell compared to Na^+ [97]. This results in higher de-solvation energies, which can influence interfacial charge-transfer kinetics. In contrast, Na^+, with its larger ionic size, tends to exhibit more flexible coordination environments and weaker interactions with solvent molecules, leading to distinct ion transport behavior [98]. Furthermore, variations in ion pairing (e.g., contact ion pairs vs. solvent-separated ion pairs) between Li^+ and Na^+ systems can significantly impact ionic conductivity and electrochemical stability. Differences in the chemistries of Li^+ and Na^+ cations also determine the composition and proportion of coordinated solvent molecules, influencing ionic mobility, ion pairing, and cation transference [99, 100]. For instance, the EC/EMC ratio in the Li^+ solvation sheath is reported to be higher than in Na-based systems, reflecting the larger size and weaker cation–solvent interactions of Na^+ ion, which diminish geometric effects. This difference significantly affects SEI layer composition and structure, interfacial kinetics, and safety-related risks under thermal or fire conditions, ultimately dictating overall battery performance [101–105]. Taken together, these considerations highlight the critical role of solvation structures in the design of high-performance LIBs and SIBs, as well as in understanding their transport and electrochemical behavior, given the distinct physicochemical properties of Li^+ and Na^+ cations.

4.3 | Cation Chemistry–Driven Electrolyte Stability

The chemical stability of carbonate components of the interphase directly influences its thickness, uniformity, and insulating properties, which in turn determine how effectively it suppresses electron diffusion through localized states and sustains long-term cyclability (Figure 8). This thermal stability could be attributed to the solubility of metastable SEI/CEI species and/or their reactions with traces of water, moisture, and alcohol impurities. Song et al. [98]. investigated the temperature-induced chemical stability of 0.5 M APF_6 (A = Li or Na) in EC-EMC (3:7, v/v) electrolytes stored at temperatures mimicking SEI decomposition conditions (i.e., 80°C). The results indicate that, although both electrolytes undergo decomposition reactions, the decomposition of the PF_6^- anion is suppressed when Li^+ is replaced with Na^+ cation. Because of its larger size and lower charge density, the $Na^+\cdots PF_6^-$ ion pair is more associated in EC-EMC media, which hinders the attack of protonic impurities toward the PF_6^- anions (Equation 1 in Figure 8). The impact of protonation on the thermodynamic stability of F^-–Lewis acid adducts (e.g., BF_4^- and PF_6^-) has been described in detail in previous articles [106, 107]. This difference in the degree of decomposition can, in turn, affect the extent of acid-base reactions between Lewis acids (e.g., PF_5, HF) and Lewis bases, such as SEI components like carbonates and alkoxides. The highly acidic products generated from the decomposition of PF_6^- anions, such as PF_5, HF, and POF_3, could corrode SEI/CEI components and reduce their mechanical stability. Thermal stability of the SEI/CEI layer is crucial as it determines the onset temperature of thermal runaway of batteries and plays a critical role in ensuring safety, longevity, and reliable performance of batteries, especially under high temperature or aggressive operating conditions. This thermal stability is predominantly dependent on the nature of the SEI/CEI building compounds, and the nature and chemical stability of the employed electrolyte salt.

4.4 | Impact of Cation-Specific Electrolyte Chemistry on Current Collector Corrosion Behavior

While the anion largely governs aluminum (Al) foil stability in nonaqueous electrolytes, the cation also plays a notable role by affecting corrosion kinetics. Compared to Li-based electrolytes, Na-based electrolytes generally delay the onset of Al dissolution and produce smoother (Figure 9a–c), cleaner foil surfaces under similar conditions [e.g., 8.0 h ($NaClO_4$) vs. 0.7 h for ($LiClO_4$) at 30 μA cm^{-2}, Figure 9b] at a polarization of 4.2 V [98]. This indicates that Na^+ slows the rate of corrosion without altering the thermodynamic possibility of Al oxidation, highlighting the influence of cation identity on the interfacial electrochemical behavior and kinetic stability of Al at high potentials.

4.5 | Role of Cation Chemistry in Low-Temperature Electrolyte Behavior

Cation chemistry strongly influences the low-temperature performance of battery electrolytes. Li^+ cations, being small with high charge density, are strongly solvated in organic carbonate electrolytes, which increases viscosity and reduces ionic conductivity at low temperatures. Additionally, their bulky solvation shell leads to slow diffusivity and a lower cation transference number (T_{Li^+} = 0.2–0.4), limiting the fraction of electric currents carried by Li^+ ions. The solvated sheath at lower temperatures becomes more stable and less prone to de-solvation, which further impedes the migration of Li^+ ions. A lower cation selectivity causes higher overpotentials and sluggish electrode kinetics, accounting for premature cell failure in lithium systems [108–111]. In contrast, Na^+ cations, being larger and weaker solvated [112], retain higher mobility in similar solvents, which can relatively preserve low-temperature ionic conductivity and transference number (T_{Na^+} = 0.4–0.5) [113]. For example, formulating high-concentration electrolytes can inhibit the movement of anions by altering the solvation structure of Na^+, thereby increasing the selectivity of cation transport [114]. Thus, the choice of cation affects not only the electrolyte's physical properties but also overall battery efficiency in low-temperature environments, with Na^+ generally offering better ionic transport under subzero conditions, while Li^+ suffers more from solvation-induced sluggishness [8, 115].

5 | Cation Chemistry–Informed Interface/Interphase Design

Interphases and interfaces play a central role in governing battery performance, with their characteristics being highly dependent on the cation involved and the overall chemical environment [116–118]. In electrochemical systems, the concepts of interphases and interfaces are distinct, each with a unique role.

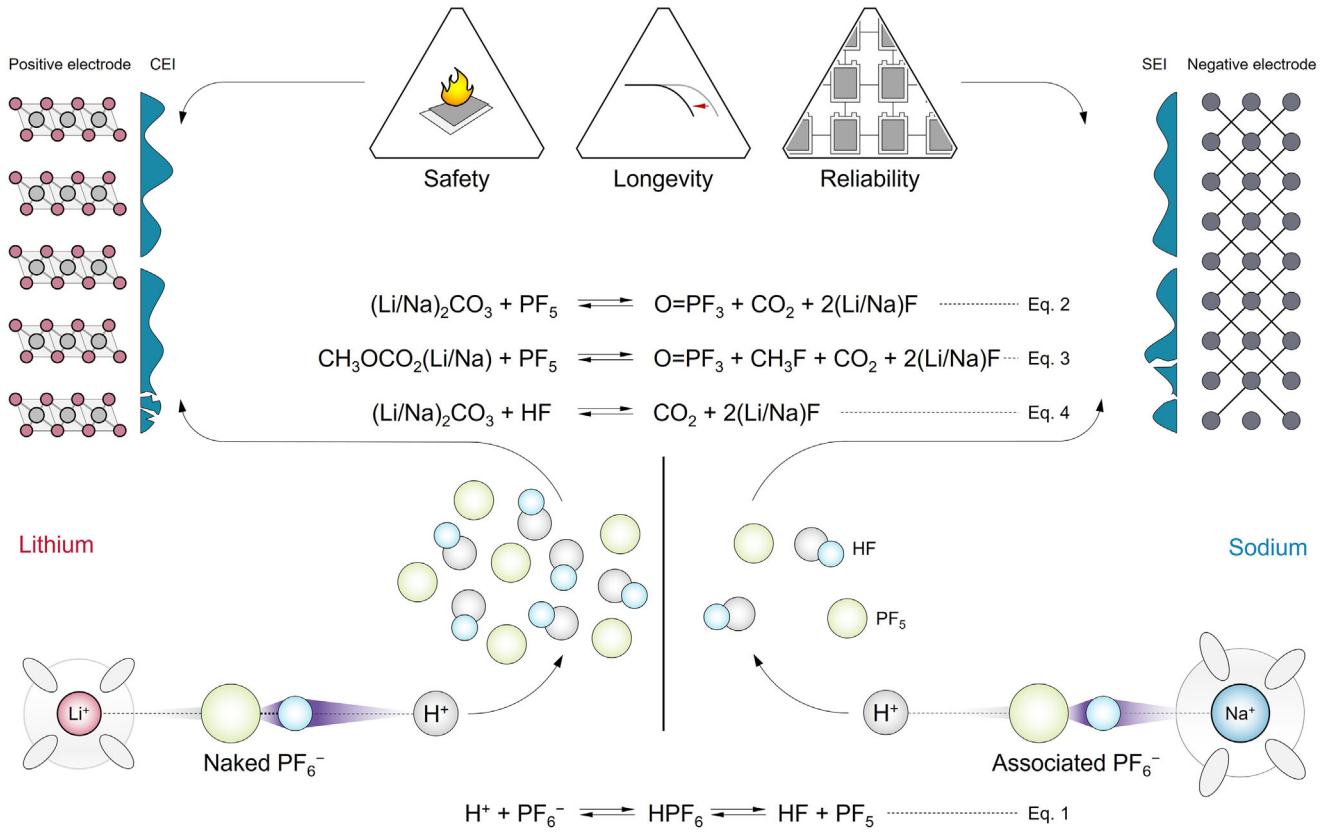

FIGURE 8 | Schematic diagram of electrolyte stability and its decomposition behaviors in Li- and Na-based systems, respectively.

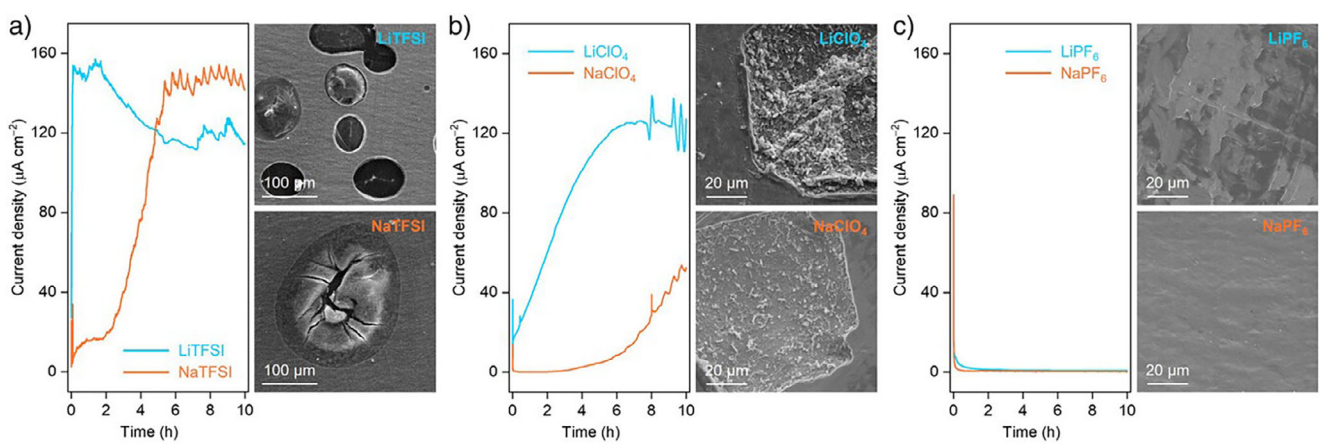

FIGURE 9 | The interfacial compatibility of Na- and Li-based electrolytes with Al foil. (a–c) Chronoamperometry curve and SEM images of the aluminum foils obtained from DC polarization measurements with different electrolyte: (a) TFSI-based systems, (b) ClO_4-based systems, and (c) PF_6-based systems. Reproduced with permission [98]. Copyright 2025, The Authors.

An 'interFACE' is a two-dimensional (thickness < 1 nm) region at the electrode's solid surface where ionic double layers form during polarization and where the immediate layer of counter-ions from the electrolyte resides. It also refers to the boundary between electrode–electrolyte interphase (EEI) components, such as between Li_2CO_3/Na_2CO_3 and LiF/NaF. In contrast, an 'interPHASE' is a three-dimensional (3D), multi-mosaic layer that occupies defined volume and exhibits ion diffusivity, microscopic structure, and chemical composition distinctly different from those of the polarized electrode, electrolyte, and/or the electrode–electrolyte interface [2, 116]. The 3D interphases in the vicinity of the electrodes and electrolytes govern the Coulombic efficiency, long-term cyclability, rate capability, safety, and cost factor of the battery cell. The 2D interfaces between electrode active materials and electrolytes, on the other hand, are the only dedicated sites for charge and mass transfer to occur. The quality of the interphase, and consequently the performance of the battery, heavily relies on its chemical composition, and this impacts ionic

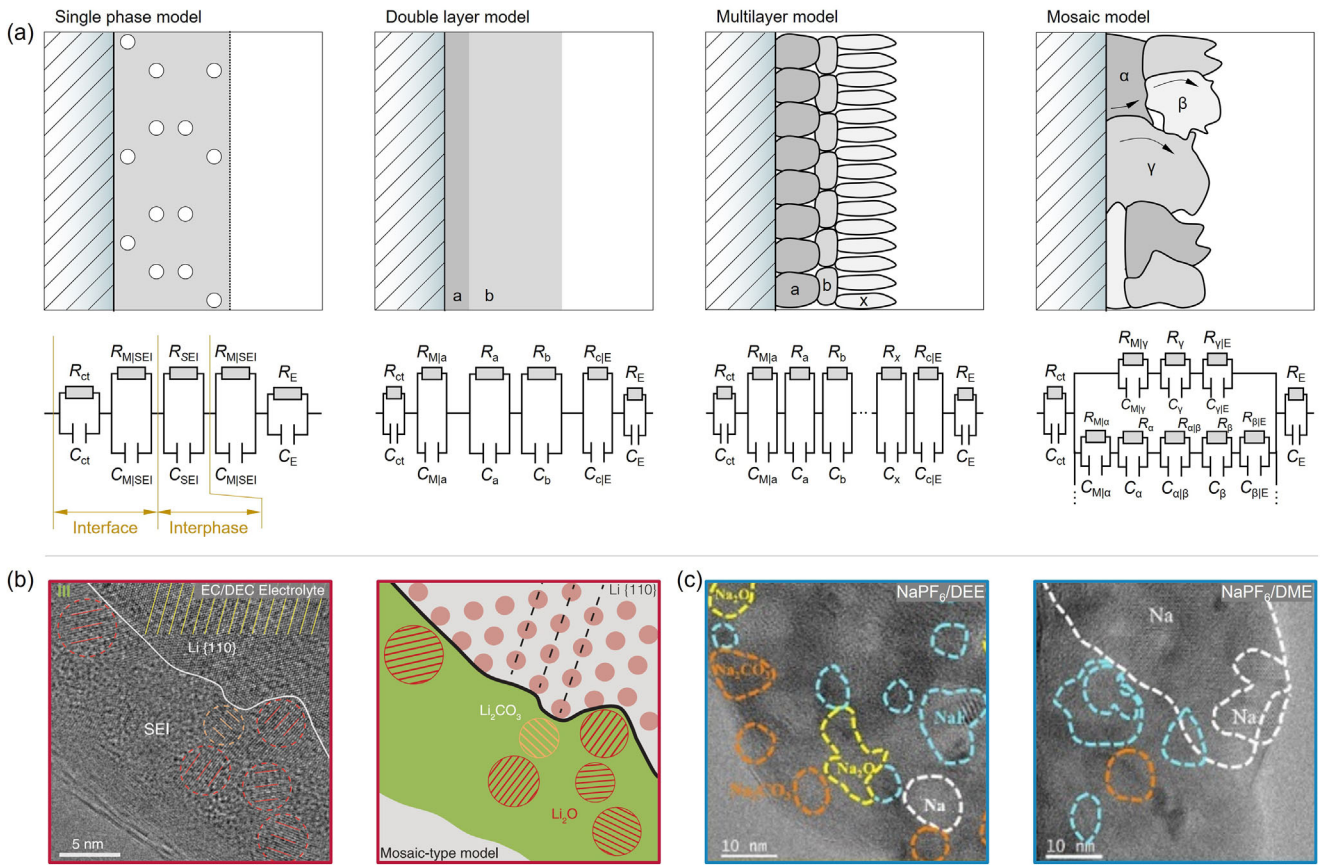

FIGURE 10 | A schematic diagram of the SEI layers in both Na and Li systems. (a) various models for the SEI layer and corresponding equivalent circuit. (b) Atomic resolution image of the interface between Li metal and the SEI, and schematic description of the observed mosaic-type structure in EC/DEC electrolyte [119]. (c) Cryo-TEM images reveal the composition of the SEI formed in electrolytes comprising $NaPF_6$ dissolved in either DEE or DME. Reproduced with permission [9]. Copyright 2023, Wiley-VCH GmbH.

conductivity, electronic insulation, mechanical stability, chemical and electrochemical stability, uniformity (homogeneity), and overall structure-composition-function properties.

In both Li- and Na-based cases, the SEI layer is considered to have a mosaic nanocomposite structure composed of an organic [CH_2OCO_2Li/Na, $ROCO_2Li/Na$ (R = CH_3, C_2H_5), ROLi/Na, etc., where R depends on the solvent] outer layer and inner inorganic [$Li(Na)_2CO_3$, Li (Na)F, $Li(Na)_2O$, $Li(Na)_2S$, and Li $(Na)_3N$, etc.] components (Figure 10a). However, the SEI formed on Na-based materials is generally more porous and mechanically less stable than that on Li-based materials (Figure 10b,c). These differences can significantly influence the various desirable properties of the interphases, as summarized below.

In both Li- and Na-based battery systems, the SEI has been far more extensively studied than the cathode–electrolyte interphase (CEI), primarily because the SEI critically governs anode stability, electrochemical performance, and overall battery safety. Consequently, research has focused heavily on its formation pathways, role in suppressing dendritic growth and its impact on electrochemical performance. The CEI, in contrast, has historically received less attention, as its impact on immediate safety is less pronounced. It is generally thinner, more heterogeneous, and composed of oxidation products such as organic carbonates, phosphates, and cathode-derived species. Notably, CEI characteristics differ between Li- and Na-based systems. In Li-based batteries, the CEI is relatively more stable, dense, poorly soluble, and compact due to stronger interaction between Li^+ and electrolyte decomposition products, whereas in Na-based batteries, the CEI tends to be less dense, more porous, more dynamic, thicker and less uniform and often partially soluble [120]. This results in slower Na^+ transport, lower electrochemical stability, and greater susceptibility to dissolution or reformation during cycling. These differences arise primarily from the larger ionic radius and weaker binding of Na^+, making the CEI less protective than in Li-based batteries.

5.1 | Mechanical Stability of the EEI Layer in Li vs. Na Systems

The mechanical stability of the Electrode-Electrolyte Interphase (EEI) in general and the SEI layer in particular are critical for curtailing battery capacity fade, as rupture of the SEI layer triggers continuous consumption of inventory metal ions (e.g., Li^+, Na^+), leading to electrolyte depletion and increased cell resistance during the creation of newly formed SEI layers [121, 122]. Thus, the SEI must be mechanically robust, but without losing flexibility to withstand large volumetric changes, during long-term cycling or calendar aging, and this heavily depends on its composition, structure, and elasticity. Na-based SEI is

generally less compact, more soluble, and mechanically weaker than Li-based SEI. According to the Hard–Soft Acid–Base (HSAB) principle, the weaker interaction of the "softer" Na^+ with hard anions (like CO_3^{2-}, F^-) in the SEI makes Na-based SEI more prone to dissolution than that of Li-based SEI. Since SEI is a heterogeneous mosaic structure composed of organic, and inorganic, with crystalline or possibly amorphous phases, its effective elastic modulus, which matters for accommodating volume changes, tends to be dominated by the softer organic/amorphous parts rather than the stiff crystalline inclusions [123–125]. This is because the SEI should endow a balance between rigidity (to resist deformation, dendrite intrusion) and flexibility (to accommodate volume changes during charging/discharging). All these imply that the interphases in Na-based batteries are less mechanically stable than their Li-based counterparts and are linked to the nature of the cation-induced structure-properties. The Pilling–Bedworth (P–B) [126] ratio indicates how well a surface layer covers the underlying metal, with values around 1–2 defining the effective range for dense, mechanically stable SEI layers. In LIBs, inorganic and organic SEI components naturally combine to give an effective P–B ratio near 1–2, resulting in a compact, self-passivating SEI that limits electrolyte decomposition and enables high Coulombic efficiency. Na, however, forms SEI components with P–B ratios often too low or too high, producing a fragile, porous layer prone to cracking and regrowth, which reduces cycle life. Fluorinated electrolytes (e.g., FEC) preferentially form dense, fluoride-rich layers like NaF, effectively raising the SEI's P–B ratio toward 1–2 effective range, stabilizing the otherwise weak Na SEI, suppressing decomposition, and improving battery performance [8, 127, 128]. In contrast, fluorination has a smaller effect on Li batteries because their SEI is already robust.

5.2 | Ion Transport Behavior of the EEI Layer in Li vs. Na Systems

Ion transport through the electrode-electrolyte interphase (SEI/CEI layer) is an indispensable and necessary parameter as it directly dictates the cell's redox efficiency, lifespan, rate capability, and safety. The SEI/CEI, which acts as a selective gateway for ionic movement between the electrode and the electrolyte, regulates the distribution of cations (Li^+ or Na^+) within the electrode matrix [128–130]. Ion transport through the SEI/CEI layer is critically determined by the SEI/CEI composition and their spatial arrangements, thickness, and crystallography of its constituent components [131, 132].

Bulk crystalline SEI components, such as Li_2CO_3, LiF, Na_2CO_3, and NaF, often show low ionic conductivity [133–135]; for instance, LiF is essentially ionically insulating ($\sim 10^{-31}$ S/cm in pure bulk) [136]. When several inorganic constituents act in concert, their synergistic effects are expected to significantly boost ion diffusion along interfacial grain boundaries relative to diffusion in an individual bulk phase [137]. In general, effective ionic conduction in actual multi-component SEI/CEI often arises at grain boundaries, phase interfaces, and their topological distribution, defects, or amorphous/disordered regions, rather than through ideal bulk crystals. Ion transport in inorganic solids differs significantly from that in organic layers and can occur via interstitial diffusion, knock-off and vacancy mechanisms, ion exchange, concerted migration, paddle-wheel motion, and grain-boundary transport.

It has been reported that Li^+ predominantly migrates through solid or liquid hosts via a knock-off or direct hopping diffusion mechanism. In this mechanism, a Li^+ ion moves by directly displacing another Li^+ ion from its site, effectively "knocking" it off and taking its position (Figure 11) [131, 138]. This type of migration tends to be relatively fast due to the small ionic size and high mobility of Li^+. In contrast, Na^+ generally relies more on vacancy-assisted diffusion or, in some cases, also via the knock-off mechanism [11, 139]. In vacancy diffusion, Na^+ ions move by hopping into nearby vacant lattice sites within the SEI (i.e., pre-existing or dynamically formed vacancies) rather than displacing another ion (Figure 11). This mechanism is often slower compared to direct hopping because it depends on the presence and distribution of vacancies within the lattice or electrolyte. The occasional knock-off mechanism for Na^+ is less dominant due to its larger ionic radius and lower mobility. Overall, the distinct diffusion pathways and kinetic behaviors observed for Li^+ and Na^+ arise directly from their intrinsic physicochemical differences, most notably their Stokes radii, charge densities, and related ion–lattice interaction strengths.

Another important distinction between Li-based SEI/CEI and Na-based SEI/CEI may lie in their relative effectiveness at suppressing electron tunneling [140]. The heterogeneous, organic-rich, and more soluble nature of the Na-based SEI leads to a loose structure with increased effective tunneling distance and reduced dielectric barrier, thus enhancing electronic leakage and self-discharge [140]. In contrast, the smaller ionic radius of Li^+ (76 pm vs. 102 pm for Na^+) enables tight packing of inorganic-rich SEI components (e.g., Li_2CO_3, LiF), forming a dense and uniform layer. This not only shortens the effective electron tunneling path but also improves the dielectric barrier property, synergistically reducing the electron tunneling probability compared to the Na-based SEI.

5.3 | Bi-Directional Anode/SEI- Cathode/CEI Cross-Talks and Their Impacts

Subtle interactions between electrodes and interphases most often play a critical role in accelerating battery failure. This bidirectional crosstalk, encompassing both cathode-to-anode and anode-to-cathode effects, significantly influences cycle life, safety, degree of cross anode-cathode and vice-versa contamination, and other key performance metrics [141]. In the cathode-to-anode interaction, dissolved transition-metal ions (e.g., Mn^{2+}, Ni^{2+}) migrate to the anode, where they deposit as metallic or oxide nanoparticles on/into the SEI layer. These conductive particles form electron transport channels across the insulating and porous SEI [142, 143], enabling electron leakage from the anode to the SEI-electrolyte interface and kinetically further accelerating electrolyte reductive decomposition, thereby thickening the SEI layer [144]. The anode-to-cathode crosstalk, on the other hand, involves the diffusion of soluble SEI components (e.g., alkyl carbonates, sodium/lithium alkoxides) from the anode to the cathode, resulting in the formation of a resistive CEI layer that hinders cathode redox reactions. In addition, self-amplifying loops involving the shuttling of gaseous products such

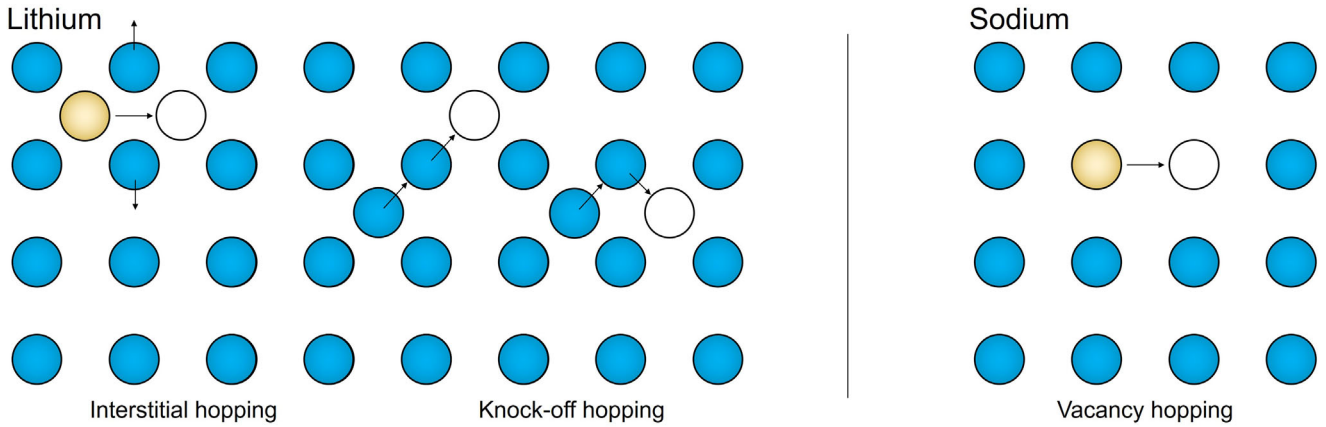

FIGURE 11 | Predominant ion conduction mechanism for Li- (left) and Na-based (right) systems.

as CO_2 and C_2H_4 between the electrodes can trigger combustion-like reactions, promote oxygen release from the cathode, and accelerate thermal runaway [145]. Due to its huge impact on battery aging, this bidirectional interaction is receiving intensive attention in Li-based batteries, but the analogue of Na has only seen sparse study. The key question is whether, or not, the cation chemistry affects the extent of electrode cross-talk and its severity in accelerating battery performance decay. Li- and Na-based batteries differ significantly in how electrode interphase cross-talk affects performance. In LIBs, the SEI is sufficiently stable, and the CEI is partially protective, which limits the migration of decomposition products and dissolved transition metals (Ni, Mn, Co) from the cathode to the anode. This results in moderate dendrite formation, slow capacity fade, and controlled impedance growth. In SIBs, the SEI and CEI are thicker, less stable, and more soluble, allowing greater anode-to-cathode and cathode-to-anode cross-talk [146, 147]. Transition metal dissolution occurs similarly in Na systems, often involving Fe and Mn, but lower-voltage cathodes may reduce dissolution rates; however, the unstable SEI can compensate, allowing metal migration to the anode. These factors collectively accelerate electrolyte decomposition, interfacial degradation, dendrite growth, and capacity fade, making Na^+ systems more sensitive to cross-talk and cycling instability compared to LIBs.

6 | Cation Chemistry-Specific Impact on Key Electrochemical Performance Metrics

6.1 | Coulombic Efficiency of Li vs. Na Battery Systems

For practical applications such as electric vehicles (EVs), renewable energy storage, and consumer electronics, both the initial Coulombic efficiency (ICE) and the overall Coulombic efficiency (CE) are critical metrics for evaluating battery performance. In full cells, ICE is widely regarded as an early predictor of long-term cycling stability, capacity retention over extended use, and the practically achievable energy density [148]. Cells with low ICE irreversibly lose a significant fraction of active lithium or sodium during the first (or initial few) cycles, primarily due to side reactions such as SEI formation and irreversible ion trapping. This loss reduces the available inventory of active ions, leading to accelerated capacity fade and ultimately limiting the practical performance and lifespan of the battery. LIBs generally exhibit high ICE (ca. 90%–96% for graphite anodes) due to efficient lithium intercalation and relatively stable SEI formation [149]. In contrast, SIBs typically show lower ICE (ca. 70%–90% for hard carbon anodes, depending on material design), because the larger Na^+ ions more easily become trapped in the porous structure of hard carbon and form less stable SEI layers. This initial loss of Na^+ in full cells reduces the effective sodium inventory, decreasing the energy density and accelerating capacity decay over repeated cycles. Recent research demonstrates that while advanced hard carbon anodes can achieve an ICE approaching 95% in laboratory conditions [150], typical practical SIBs still lag behind LIBs in ICE, which reduces the reversible capacity after formation. In summary, ICE is a crucial determinant of full-cell performance for both chemistries. LIBs benefit from higher ICE, giving them superior long-term stability, whereas SIBs require careful material and electrolyte engineering to compensate for lower ICE and the resulting irreversible Na losses.

6.2 | Rate Capability of Li vs. Na Battery Systems

Another important parameter is the rate capability (power performance) of a battery, which is governed by multiple factors, including electrode wetting, bulk electrolyte transport, interfacial and interphase kinetics, de-solvation energy, and solid-state ion transport within the electrode matrix. These factors are, in turn, strongly influenced by the nature of the cation; for instance, Li^+ and Na^+ differ in ionic radius, solvation energy, and mobility, which directly impact charge-transfer kinetics, diffusion rates, and overall cell rate performance. For instance, while Na^+ often has a lower de-solvation energy due to weaker cation–solvent interactions, facilitating faster interfacial charge transfer, Li^+ exhibits faster solid-state diffusion within electrode materials because of its smaller ionic radius. The overall rate capability is governed by the competitive interplay of ion diffusion at the interface, across the interphase, and within the bulk of active electrode materials, as well as electronic transport in the electrodes and ion transport in both the bulk electrolyte and electrolyte-filled pores [151]. The rate-determining step is dictated by the predominance of one of these processes, which in turn depends on the nature of the cation. Thus, high-rate performance relies on the concurrent

optimization of electrode particle size, electrolyte composition and concentration, interphase conductivity, electrode thickness, mass loading, surface and bulk engineering, and other material and structural parameters.

7 | Nature of Dendrites in Li and Na Battery Systems

Li and Na exhibit distinctly different dendrite formation behaviors due to their intrinsic differences in ionic size, mobility, and interfacial chemistry. Li dendrites are typically sharp, needle-like, filamentous, or tree-like structures, resulting from uneven deposition conditions, low surface diffusion, small Li^+ ion radius, and high mobility. These dendrites are highly reactive, easily penetrate separators, and pose severe safety risks, including short circuits and thermal runaway. In contrast, Na dendrites tend to be more mossy, porous, heterogeneous, and blunt, owing to the larger ionic size, higher surface mobility of Na, and slower diffusion kinetics, which promotes relatively uniform deposition. Another key distinction lies in interfacial behavior, in which Li forms a comparatively stable SEI, but its mechanical fragility leads to crack-induced dendrite growth. Na, however, forms a less stable SEI, resulting in continuous side reactions and less controlled deposition, though often with reduced sharp dendrite formation. Mechanically, Na's softer nature allows it to deform more easily, further contributing to less rigid dendritic structures compared to Li. Overall, Li dendrites are sharper and more hazardous, while Na dendrites are less aggressive in shape but more unstable over long-term cycling [152–154].

8 | Distinct Formation Processes in Li- and Na-Based Batteries

The formation process of rechargeable batteries involves sequential steps, including electrolyte wetting, controlled initial cycling, SEI/CEI formation, and aging, that critically determine electrochemical activation and long-term performance. Proper electrolyte wetting ensures complete pore infiltration and intimate electrode–electrolyte contact. Insufficient wetting can hinder ion transport and cause uneven current distribution during formation. During low-rate formation cycling, SEI forms via electrolyte reduction at the anode, while CEI develops through electrolyte oxidation at the cathode. Subsequent aging or conditioning at controlled temperature and potential stabilizes these interphases, lowers leakage currents, and improves capacity consistency.

Cation chemistry strongly influences the formation process. Li^+, with a small radius, high charge density, and high reduction potential, forms a dense, inorganic-rich SEI rapidly, enabling relatively stable interphase formation within standard formation times. In contrast, Na^+, being larger and less charged, produces thinner, more dynamic SEI layers with higher solubility, which may require longer formation and conditioning periods to achieve comparable interphase stability. These differences impact energy consumption, labor, and equipment use, making formation a significant cost driver. In LIBs, formation and aging account for ~33 % of total manufacturing cost and can take up to three weeks [155, 156]. For Na-based batteries, the dynamic SEI and slower stabilization could further extend formation time, increasing energy and capital costs.

9 | Self-Discharge Rate Comparison of Li vs. Na Systems

The self-discharge rate is a critical parameter for batteries, as it indicates how rapidly a battery loses its charge when idle. Different types of batteries exhibit varying self-discharge rates, which can significantly influence their efficiency and suitability for specific applications [157]. Self-discharge in Li- and Na-based batteries arise from parasitic reactions at the electrodes and within the interphases. In LIBs, self-discharge is generally low, typically around 1%–3% per month at room temperature, though it can reach up to ~5% in some cases during initial storage, depending on state of charge, temperature, and cell chemistry [158–162]. In contrast, SIBs often exhibit higher self-discharge, roughly 5%–10% per month [163], due to more dynamic and partially soluble SEI/CEI layers, larger electrode volume changes, and slightly lower electrolyte stability. Although quantification for Na^+ ion specifically varies with cell design and testing conditions, this broader range reflects the relatively higher self-discharge generally observed in Na-based systems compared with Li-based ones.

10 | Safety Considerations of Li vs. Na Systems

Battery researchers often prioritize the development and improvement of high-energy and power systems. However, safety remains one of the most critical performance metrics, particularly for applications such as in electric vehicles, aviation, or marine transport, where thermal stability, overcharge tolerance, and mechanical robustness are essential. While several efforts are being devoted to qualifying the safety issues of LIBs, studies dealing with SIBs are much scarcer. The safety of large-format batteries is a systemic issue influenced by multiple factors, and a comprehensive assessment requires a systematic approach, including investigations at the cell-component, cell, module, and pack levels. This section discusses the impact of cation chemistry on safety, focusing on a material-level approach with projected implications for large-format cells. Thermal instability at the cell level arises from a complex interplay of factors, including electrode decomposition, interfacial degradation, electrolyte breakdown, and structural changes.

10.1 | Thermal Stability of Battery Cell Components and SEI/CEI Layers

DSC analysis provides crucial insights into the thermal behavior of electrolytes, revealing the exothermic onset temperature associated with SEI decomposition, the peak reaction temperature, and the total heat released (Figure 12a) [164]. These parameters play an instrumental role in designing, evaluating, and selecting electrolytes with improved safety profiles. The characteristics of the SEI layer are determined by the intrinsic physico-chemical properties of both the anode and the electrolyte, and by carefully tailoring the electrolyte composition, it is possible to partially delay the onset of thermal runaway. Despite insights from the

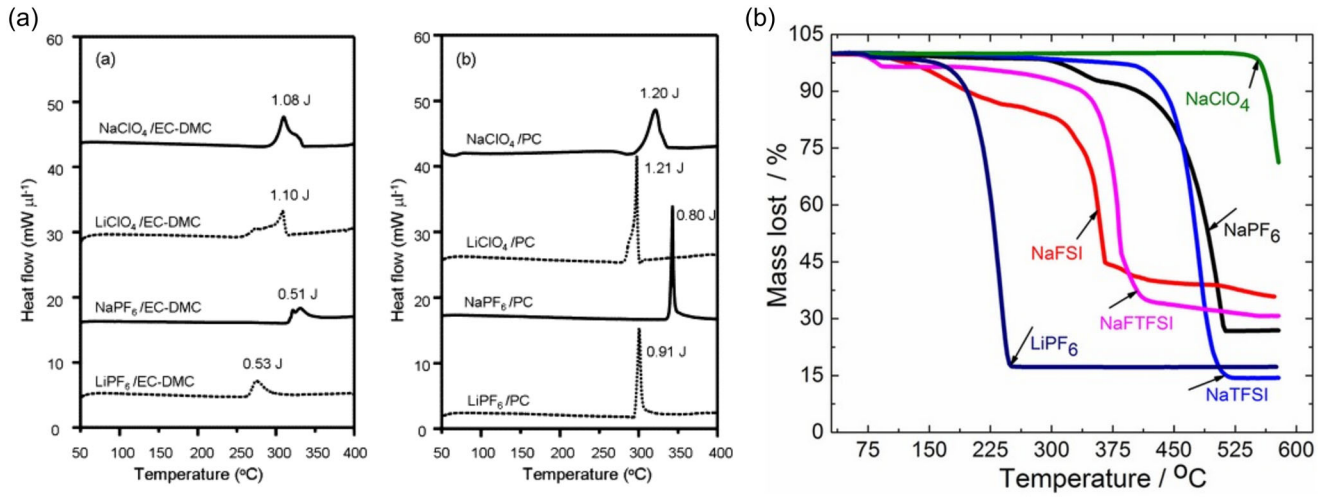

FIGURE 12 | (a) DSC curves of different electrolytes for Li- and Na-based systems. Reproduced with permission [164]. Copyright 2013, Elsevier B.V. (b) TGA curves of various conducting salt for Li- and Na-based systems. Reproduced with permission [165]. Copyright 2016, Wiley-VCH Verlag GmbH & Co. KGaA, Weinheim.

more mature Li^+ technology can guide the initial selection of candidate electrolytes, notable differences exist with distinct anode materials, the potentially higher solubility of Na-SEI compounds, and the generally higher thermal stability of Na salts relative to their Li counterparts (Figure 12b) complicate direct extrapolation of Li-based results to Na-based systems [165]. The superior stability of $NaPF_6$ entails lesser generation of highly reactive Lewis's acids such as POF_3 and HF compared to that of $LiPF_6$. On the other side, Na-SEI is more soluble than Li-SEI. Consequently, predicting the thermal runaway onset in SIBs based solely on lithium data remains challenging. Comprehensive thermal investigations, combined with a detailed characterization of SEI composition, are therefore essential for both chemistries to anticipate and control undesirable temperature-induced reactions. However, some studies reveal that the thermal runaway and decomposition behavior of the SEI breakdown occurs at lower temperatures in Na than in Li systems, contributing to higher self-heating rates in Na-based batteries [166].

Despite the anode being the starting point of thermal runaway, the cathode and its accompanying CEI also play a significant role in the eventual catastrophic safety risks of Li- and Na-based batteries [167, 168]. They drive the onset of oxygen release, lattice degradation, and ultimately thermal runaway. In this context, layered cathodes (e.g., $LiMO_2$ and $NaMO_2$) are more prone to thermal instability because deep (de)lithiation or (de)sodiation weakens metal–oxygen bonds, enabling lattice oxygen release that reacts exothermically with the electrolyte and accelerates failure. Compared to its Li counterparts, layered $NaMO_2$ such as $Na_{0.5}Ni_{0.3}Mn_{0.3}Co_{0.3}O_2$ are more vulnerable, due to inherently weaker Na–O bonds compared to Li–O bonds and greater structural distortion, which facilitate oxygen evolution at elevated temperatures (~180°C) [167]. This oxygen loss compromises the lattice structure and triggers irreversible phase transitions between 200 and 400°C. The released oxygen and volatile species can react exothermically with the electrolyte or CEI layer, significantly increasing the risk of thermal runaway [167–170]. In contrast, Li-based cathodes are more thermally robust, with decomposition typically occurring above 230°C. Their smaller Li^+ ions enable tighter atomic packing, denser oxygen sublattices, and stronger cationic interactions, which collectively reinforce the TM–O framework and enhance lattice rigidity.

By contrast, polyanionic cathodes with an electron-withdrawing PO_4^{3-} group exhibit superior safety, where strong covalent bonds suppress oxygen evolution and limit heat generation compared to layered cathode materials. However, the influence of the cation remains striking, as $NaFePO_4$-based electrodes generate markedly more heat than their $LiFePO_4$ counterparts, highlighting the greater thermal sensitivity of Na-based systems [171]. This is mainly due to slower ion transport $NaFePO_4$ which increases internal resistance and polarization, producing more Joule (resistive) heating.

Regarding interphase contributions, the SEI formed on the anode is thermally fragile and typically decomposes first at relatively low temperatures, exposing reactive electrode surfaces and initiating heat generation, serving as the trigger for thermal runaway. In contrast, the CEI on the cathode plays a more prominent role at elevated temperatures. Thus, while the SEI drives the onset of thermal instability, the CEI dictates its severity and propagation. Li-CEIs are generally more stable and protective than Na-CEIs, although CEI stability in both chemistries strongly depends on the cathode material.

In summary, similar to Li-based systems, the safety of Na-based cathode materials is influenced by multiple mechanisms: phase transitions at elevated temperatures and oxygen-rich redox reactions; self-heating coupled with layer gliding in layered oxides (MO_2); Mn disproportionation and the Jahn-Teller effect in tunnel-type oxides; CEI decomposition in polyanionic cathodes containing PO_4^{3-}, SO_4^{2-}, $P_2O_7^{4-}$, or BO_3^{3-}; and desorption of crystallized or coordinated water, along with phase transitions, in Prussian blue analogues $(Na_xM[Fe(CN)_6]_{1-y}\cdot\square_y\cdot zH_2O$, where $\square$ represents $[Fe(CN)_6]$ vacancies and M is a transition metal such as Fe, Mn, Ni, or Co) [172].

10.2 | Safety Implications of Zero-Volt Storage in SIBs

Discharging LIBs to 0 V risks copper current collector dissolution, as its oxidation occurs above 3.5 V vs. Li/Li^+. Flügel et al. [173] observed holes in 18650 LIBs collectors after holding it at 0 V for 430 h, and recharging can produce copper dendrites, promoting internal short circuits and thermal runaway. In contrast, SIBs, which use aluminum collectors, remain stable under full discharge to 0 V, as demonstrated by Rudola et al. [82] for a 5.5 mAh Na^+ pouch cell. This highlights how the cation chemistry impacts the choice of current collector material and electrochemical potential windows, and these in turn determine the risk of degradation and associated safety hazards. Therefore, SIBs offer enhanced safety during shipment and long-term storage.

10.3 | Combustion and Fire-Induced Toxicity

Another key aspect of battery safety assessment involves the evaluation of both thermal and chemical hazards that may arise during combustion [174]. Battery electrolytes are typically formulated from a combination of flammable linear carbonates (di-alkyl carbonates with methyl and/or ethyl groups) and combustible cyclic carbonates, such as ethylene carbonate (EC) or propylene carbonate (PC), which together provide the desired ionic conductivity, electrochemical stability, and optimized interphases. Overall, the heat release rate (HRR) is largely determined by the choice of solvents, with inorganic Li or Na salts having a comparatively minor effect, whereas the composition of emitted gases is influenced by the combined chemistry of both solvents and salts. Guy et al. [175] demonstrated that Na-based NP30 ($NaPF_6$ in EC/DMC) electrolytes emit significantly less HF and POF_3 than Li-based LP30 (Figure 13), regardless of ventilation conditions, indicating that gas formation is largely independent of combustion intensity and relies on the cation chemistry. The emissions result from the thermal decomposition of the salts to PF_5, followed by hydrolysis with water produced during carbonate solvent combustion. HF is released early, while POF_3 appears later. Further hydrolysis of POF_3 can produce additional phosphorus-containing compounds (HPO_2F_2, H_2PO_3F, H_3PO_4) along with more HF; however, after combustion, the limited availability of water restricts these reactions, leaving POF_3 and HF as the primary detectable gases. These results highlight the relative safety advantage of Na electrolytes in terms of corrosive gas generation during combustion.

11 | Drop-in Compatibility of SIBs: Implications on Manufacturing

In the literature, SIBs are often assumed to be directly drop-in compatible with existing Li-ion manufacturing infrastructure, implying immediate high-yield production without process modifications [15]. However, the question remains: how seamless is this assumption in practice? To critically evaluate such generalized claims, it is important to unpack the various factors that influence manufacturing compatibility. Key aspects include differences in electrode materials, electrolyte characteristics, voltage windows, and thermal and mechanical behaviors. For instance, differences in slurry rheology of cathode materials can affect calendaring and drying, while particle size sensitivity may necessitate adjustments in milling or coating parameters. On the anode side, graphite is optimized for LIBs, whereas SIBs typically use hard carbon, which differs in slurry viscosity, particle size distribution, and binder requirements, impacting electrode coating, drying, and calendaring processes. Besides, hard carbon is abrasive for the coaters. Variations in voltage windows influence cell balancing, formation protocols, and energy density optimization. Additionally, the larger ionic radius of sodium may require modifications to electrode and cell stack design, including the need for thicker current collectors or adjusted calendaring pressures to prevent cracking. Overall, although SIBs can be conceptually considered "drop-in" in using the same characterization techniques, equipment, and machine, these subtle but significant differences in materials, electrolyte handling, formation protocols, and thermal/mechanical behavior necessitate a transitional phase [176]. During this phase, processes must be optimized, production lines adapted, operators retrained, and quality control (QC) tuned to sodium-specific requirements. In short, although SIBs can conceptually leverage existing Li^+ ion manufacturing lines, they are not instant plug-and-play technologies, and practical adaptation is necessary.

12 | Conclusions

This Perspective delves into the divergences of Na^+ and Li^+ cation chemistry by revisiting the bonding concepts and ionic solutions, which are well established in modern chemistry. Pitfalls, myths, and misconceptions arising from the reliance on Li^+ design principles are elaborated, along with applied settings to counteract these dilemmas. Building on meticulous examination of fundamental differences in the cation chemistry, recent literature reports, and our insights and thought-provoking accumulations in this domain, the following conclusions and future direction can be taken.

1. Conceptually, the chemical characteristics of Na^+ cations are very relevant to those of Li^+ cations, but at the same time, are endowed with several distinctions that can significantly impact the design of Na-based active electrode materials, electrolytes, polymeric binders, interphases/interfaces, safety, and optimization of accompanying protocols. The concept of ion radius itself conveys the coordination environment, kinetics, and compatibility of Na^+ cations with host materials; thus, such a concept should be carefully evaluated while designing highly conductive Na-based electrolytes, electrodes, and interphases. Open-ended questions related to this could be: are solvated Na^+ cations categorically smaller than solvated Li^+ cations in aprotic solvents? How does ion size affect their transport behavior in bulk electrolyte and at the electrode-electrolyte interphases/interfaces? In this direction, the thermodynamic concepts established in "host-guest chemistry" can be transferred into battery electrolyte and interfacial designs.
2. For electrode materials, the larger ionic radius, low ionic potential, and distinct polarizability of Na^+ alter intercalation/deintercalation mechanisms, structural evolution, and cycling stability, necessitating the development of

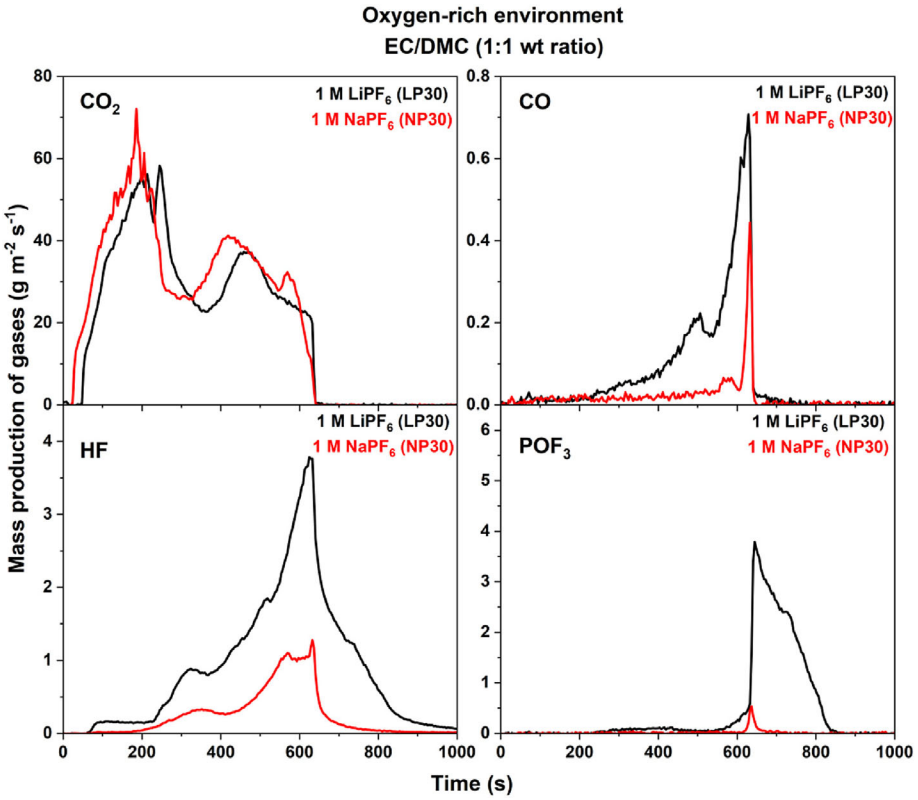

FIGURE 13 | Gases released during combustion of LP30 and NP30 electrolytes under an oxygen-lean environment. Reproduced with permission [175]. Copyright 2024, The Authors.

Na^+-specific host structures rather than simple adaptations of LIB systems. For positive electrodes, the preferred oxygen stacking type in layered metal oxides depends on the ratio of the A^+ cation to the transition metal cation radius, in that larger A^+/M ratios favor octahedral coordination (O-type) for Na systems. For negative electrodes, Na alloys are limited to special hosts that can structurally and energetically accommodate their larger size, while classic Li alloys are versatile due to favorable thermodynamics and fast kinetics.

3. The quality of electrolyte-electrode interphases (SEI/CEI) in Na-based batteries is inherently inferior to their counterparts in LIBs. The high solubility of Na-SEI building materials leads to a less mechanically stable, porous, and inhomogeneous SEI layer, ultimately resulting in low initial coulombic efficiency, high self-discharge, thermally unstable, energy-intensive formation process of SIBs. Differing from the Li^+ transport in SEI/CEI layers, Na^+ generally relies more on vacancy-assisted diffusion and less on the knock-off mechanism due to its larger ionic radius and lower mobility. Fluorinated compounds (e.g., FEC) have a huge effect in balancing the too low or too large Pilling–Bedworth (P–B) ratio and present a stronger effect on Na systems than in LIBs. Thus, designing an effective fluoride-rich SEI layer is more critical for Na systems to mitigate the anode-to-cathode and cathode-to-anode cross-talks.

4. The distinct cation chemistry of Li^+ and Na^+ governs interfacial behavior across dendrite formation, cell formation, and aging, and self-discharge. Li^+, with its smaller size and higher charge density, tends to form sharp, filamentous dendrites and a dense, inorganic-rich SEI that stabilizes relatively quickly. In contrast, Na^+ promotes more mossy dendrites and forms a more dynamic SEI, requiring extended formation and conditioning steps to achieve stabilization, thereby increasing overall costs. These interfacial differences also impact performance, as the less stable SEI in Na systems leads to higher parasitic reactions and consequently higher self-discharge.

5. From a safety perspective, SIBs present both advantages and disadvantages, demanding further appraisal. In general, the thermal instability of the SEI and CEI layers is higher in SIBs, and breakdown at lower temperatures than in Li-based systems, contributing to higher self-heating. Although the contribution of cathode materials to thermal instability occurs at later stages relative to the anode and SEI layer, Na-based cathodes generally display lower thermal stability than their Li^+ ion counterparts. On the contrary, SIBs are generally considered safer from a fire-induced hazard perspective. From a safety perspective in shipment and storage, SIBs have been shown to be safely discharged down to 0 V (true 0% state of charge) and even beyond, including into reverse polarity (negative voltages), providing an additional safety advantage. Therefore, a thorough and accurate assessment of SIBs safety is essential, accounting for both seemingly contradictory yet complementary factors that together define the batteries' overall safety profile.

6. Regarding the drop-in feasibility, although SIBs can in principle be processed on existing Li-ion production lines, the differences in electrode materials, electrolyte behavior,

voltage profiles, and mechanical expansion require targeted adjustments in coating, calendaring, formation, and quality control. As a result, SIBs are far from a true plug-and-play technology and demand careful, conscious assessment of the whole value-chain manufacturing processes while attempting to scale up.

In summary, SIBs stand as promising power sources for building more eco-friendly, cost-effective, and technologically sustainable energy networks, thanks to extremely abundant resources and manufacturing processes akin to today's LIBs. This is of particular importance given the burgeoning application scenarios of electrochemical energy storage devices, together with the ever-expanding demands from EVs, grid storage, and humanoid systems. However, advancing these technologies demands recognizing and leveraging cation-specific characteristics and unique differences between Li^+ and Na^+ as they play a pivotal role in designing and optimizing electrode materials, electrolytes, and interphases, and ultimately unlocking the full potential and practical deployment of sodium-based batteries for large-scale applications. Finally, yet critically, in-depth system-level considerations are required while attempting to holistically comprehend the impact of cation chemistry, as it influences every stage of the battery development value chain, from atomic and material scales to the fully assembled cell, module, and pack.

Acknowledgements

This work is financially supported by the National Natural Science Foundation of China (Nos. 22279037 and 52203223), and the Fundamental Research Funds for Central Universities, HUST (No. 2020kfyXJJS095). This project is supported by the Huazhong University of Science and Technology (HUST) and the RWTH Aachen University Seed Fund Project (No. 5003013164). S. P. kindly acknowledges the basic funding oh the Helmholtz Association.

Open access funding enabled and organized by Projekt DEAL.

Conflicts of Interest

The authors declare no conflicts of interest.

Data Availability Statement

The data that support the findings of this study are available from the corresponding author upon reasonable request.

References

1. M. Khaleel, Z. Yusupov, H. Kilic, et al., "Battery Technologies In Electrical Power Systems: Pioneering Secure Energy Transitions," *Journal of Power Sources* 653 (2025): 237709, https://doi.org/10.1016/j.jpowsour.2025.237709.

2. H. Zhang, L. Qiao, H. Kühnle, E. Figgemeier, M. Armand, and G. G. Eshetu, "From Lithium to Emerging Mono-and Multivalent-Cation-Based Rechargeable Batteries: Non-Aqueous Organic Electrolyte and Interphase Perspectives," *Energy & Environmental Science* 16 (2023): 11–52, https://doi.org/10.1039/d2ee02998g.

3. B. Ramasubramanian, R. Prasada Rao, G. K. Dalapati, S. Adams, and S. Ramakrishna, "Sustainable Materials and Decarbonization Prospects in Battery Technologies," *ACS Applied Energy Materials* 7 (2024): 3018–3020, https://doi.org/10.1021/acsaem.4c00821.

4. D. Larcher and J. M. Tarascon, "Towards Greener and More Sustainable Batteries for Electrical Energy Storage," *Nature Chemistry* 7 (2015): 19–29, https://doi.org/10.1038/nchem.2085.

5. J. Y. Hwang, S. T. Myung, and Y. K. Sun, "Sodium-Ion Batteries: Present and Future," *Chemical Society Reviews* 46 (2017): 3529–3614, https://doi.org/10.1039/c6cs00776g.

6. X. X. He, L. Li, X. Wu, and S. L. Chou, "Sustainable Hard Carbon for Sodium-Ion Batteries: Precursor Design and Scalable Production Roadmaps," *Advanced Materials* 37 (2025): 2506066, https://doi.org/10.1002/adma.202506066.

7. S. Zhou, X. Chen, X. Zhang, et al., "Recent Progress on Organic Liquid Electrolyte for High-Temperature Sodium Batteries," *Advanced Functional Materials* 35 (2025): 2418784, https://doi.org/10.1002/adfm.202418784.

8. T. Deng, C. Li, G. Lu, Z. Li, C. Xu, and R. Wang, "Accelerating Interfacial Desolvation Kinetics Using NaF-Rich Composite Sodium for High-Performance All-Climate Sodium–Metal Batteries," *Energy & Environmental Science* 18 (2025): 3278–3287, https://doi.org/10.1039/d4ee05369a.

9. S. Wang, S. Weng, X. Li, et al., "Unraveling the Solvent Effect on Solid-Electrolyte Interphase Formation for Sodium Metal Batteries," *Angewandte Chemie* 62 (2023): 202313447, https://doi.org/10.1002/anie.202313447.

10. Y. Li, S. Kumar, G. Yang, et al., "The Contrast Between Monovalent and Multivalent Metal Battery Anodes," *Science* 389 (2025): adl5482, https://doi.org/10.1126/science.adl5482.

11. Y. Wang, J. Ouyang, H. Yuan, et al., "Impact of Local Amorphous Environment on the Diffusion of Sodium Ions at the Solid Electrolyte Interface in Sodium-Ion Batteries," *Chinese Chemical Letters* 36 (2025): 110412, https://doi.org/10.1016/j.cclet.2024.110412.

12. O. Zhanadilov and S. T. Myung, "All-Anion Electrolyte Solutions for High-Potential Sodium Batteries," *Nature Nanotechnology* 20 (2025): 327–328, https://doi.org/10.1038/s41565-025-01869-5.

13. H. Zhu, L. Peng, J. Wu, et al., "Fluorine-Doped Micropore-Covered Mesoporous Carbon Nanofibers for Long-Lasting Anode-Free Sodium Metal Batteries," *Nature Communications* 16 (2025): 5494, https://doi.org/10.1038/s41467-025-60168-8.

14. Z. Cui, C. Liu, and A. Manthiram, "A Perspective on Pathways Toward Commercial Sodium-Ion Batteries," *Advanced Materials* 37 (2025): 2420463, https://doi.org/10.1002/adma.202420463.

15. A. Yao, S. M. Benson, and W. C. Chueh, "Critically Assessing Sodium-Ion Technology Roadmaps and Scenarios for Techno-Economic Competitiveness Against Lithium-Ion Batteries," *Nature Energy* 10 (2025): 404–416, https://doi.org/10.1038/s41560-024-01701-9.

16. R. J. Boyd, "The Relative Sizes of Atoms," *Journal of Physics B: Atomic and Molecular Physics* 10 (1977): 2283–2291, https://doi.org/10.1088/0022-3700/10/12/007.

17. Y. Marcus, "Ionic Radii in Aqueous Solutions," *Chemical Reviews* 88 (1988): 1475–1498, https://doi.org/10.1021/cr00090a003.

18. B. Cordero, V. Gomez, A. E. Platero-Prats, et al., "Covalent Radii Revisited," *Dalton Transactions* (2008): 2832, https://doi.org/10.1039/b801115j.

19. G. V. Gibbs, O. Tamada, and M. B. Boisen Jr, "Atomic and Ionic Radii: A Comparison With Radii Derived From Electron Density Distributions," *Physics and Chemistry of Minerals* 24 (1997): 432–439, https://doi.org/10.1007/s002690050057.

20. W. L. Bragg, "XVIII. The Arrangement of Atoms in Crystals," *The London, Edinburgh, and Dublin Philosophical Magazine and Journal of Science* 40 (1920): 169–189, https://doi.org/10.1080/14786440808636111.

21. J. C. Slater, "Atomic Radii in Crystals," *The Journal of Chemical Physics* 41 (1964): 3199–3204, https://doi.org/10.1063/1.1725697.

22. G. F. Hüttig, "Beiträge Zur Systematischen verwandtschaftslehre. XVI. Über die Ammoniakate der Calciumhalogenide," *Zeitschrift für*

Anorganische Und Allgemeine Chemie 114 (1920): 24–26, https://doi.org/10.1002/zaac.19201140103.

23. G. F. Hüttig, "Zur Geometrie der Koordinationszahl. II," *Zeitschrift für Anorganische Und Allgemeine Chemie* 142 (1925): 135–142, https://doi.org/10.1002/zaac.19251420113.

24. R. D. Shannon, "Revised Effective Ionic Radii and Systematic Studies of Interatomic Distances in Halides and Chalcogenides," *Acta Crystallographica Section A* 32 (1976): 751–767, https://doi.org/10.1107/s0567739476001551.

25. W. P. Davey, "The Radii of Atoms and Ions," *Chemical Reviews* 2 (1925): 349–367, https://doi.org/10.1021/cr60007a003.

26. R. Khatiwada and P. Li, "Deciphering Atomic Polarizability: The Absolute Radii and Orbital Contributions Visited," *The Journal of Physical Chemistry A* 129 (2025): 5118–5126, https://doi.org/10.1021/acs.jpca.5c02786.

27. V. M. Goldschmidt, "Über Atomabstände in Metallen," *Zeitschrift für Physikalische Chemie* 133U (1928): 397–419, https://doi.org/10.1515/zpch-1928-13327.

28. L. Pauling, "The Sizes Of Ions And The Structure Of Ionic Crystals," *Journal of the American Chemical Society* 49 (1927): 765–790, https://doi.org/10.1021/ja01402a019.

29. M. Smith, Z. Li, L. Landry, K. M. Merz, and P. Li, "Consequences of Overfitting the van der Waals Radii of Ions," *Journal of Chemical Theory and Computation* 19 (2023): 2064–2074, https://doi.org/10.1021/acs.jctc.2c01255.

30. M. Della Monica and L. Senatore, "Solvated Radius of Ions in Nonaqueous Solvents," *The Journal of Physical Chemistry* 74 (1970): 205–207, https://doi.org/10.1021/j100696a037.

31. K. Hayamizu, Y. Chiba, and T. Haishi, "Dynamic Ionic Radius of Alkali Metal Ions in Aqueous Solution: A Pulsed-Field Gradient NMR Study," *RSC Advances* 11 (2021): 20252–20257, https://doi.org/10.1039/d1ra02301b.

32. C. C. Miller, "The Stokes-Einstein Law for Diffusion in Solution," *The Royal Society* 106 (1924): 724–749, https://doi.org/10.1098/rspa.1924.0100.

33. G. G. Stokes, "On the Effect of the Internal Friction of Fluids on the Motion of Pendulums," *Mathematical and Physical Papers* (Cambridge University Press, 1851), 1880–1905.

34. A. Baer, S. E. Wawra, K. Bielmeier, et al., "The Stokes–Einstein–Sutherland Equation at the Nanoscale Revisited," *Small* 20 (2024): 2304670, https://doi.org/10.1002/smll.202304670.

35. A. Einstein, "Über die von der Molekularkinetischen Theorie der Wärme Geforderte Bewegung von in Ruhenden Flüssigkeiten Suspendierten Teilchen," *Annalen der Physik* 322 (1905): 549–560, https://doi.org/10.1002/andp.19053220806.

36. W. Sutherland, "LXXV. A Dynamical Theory of Diffusion for Non-Electrolytes and the Molecular Mass of Albumin," *The London, Edinburgh, and Dublin Philosophical Magazine and Journal of Science* 9 (1905): 781–785, https://doi.org/10.1080/14786440509463331.

37. W. Zhang, Y. Liu, and Z. Guo, "Approaching High-Performance Potassium-Ion Batteries via Advanced Design Strategies and Engineering," *Science Advances* 5 (2019): aav7412, https://doi.org/10.1126/sciadv.aav7412.

38. M. Lu, Y. Yan, Y. Zheng, et al., "Recent Advances of Aqueous Rechargeable Lithium/Sodium Ion Batteries: Key Electrode Materials and Electrolyte Design Strategies," *Materials Today Energy* 38 (2023): 101454, https://doi.org/10.1016/j.mtener.2023.101454.

39. J. Lai, Y. Xing, N. Chen, L. Li, F. Wu, and R. Chen, "Electrolytes for Rechargeable Lithium–Air Batteries," *Angewandte Chemie International Edition* 59 (2020): 2974–2997, https://doi.org/10.1002/anie.201903459.

40. Y.-S. Hu and H. Pan, "Solvation Structures in Electrolyte and the Interfacial Chemistry for Na-Ion Batteries," *ACS Energy Letters* 7 (2022): 4501–4503, https://doi.org/10.1021/acsenergylett.2c02529.

41. Y. Taji, A. Zagalskaya, I. Evazzade, et al., "Alkali Metal Cations Change the Hydrogen Evolution Reaction Mechanisms at Pt Electrodes in Alkaline Media," *Nano Materials Science* 7 (2025): 729–734, https://doi.org/10.1016/j.nanoms.2022.09.003.

42. Y. Marcus, "Are Ionic Stokes Radii of Any Use?," *Journal of Solution Chemistry* 41 (2012): 2082–2090, https://doi.org/10.1007/s10953-012-9922-4.

43. L. Pauling and G. W. Wheland, "The Nature of the Chemical Bond. V," *The Journal of Chemical Physics* 2 (1934): 482, https://doi.org/10.1063/1.1749514.

44. L. Pauling, *The Nature of the Chemical Bond and the Structure of Molecules and Crystals: An Introduction to Modern Structural Chemistry* (Cornell University Press, 1960).

45. L. Pauling, "The Nature of the Chemical Bond. IV. The Energy Of Single Bonds And The Relative Electronegativity of Atoms," *Journal of the American Chemical Society* 54 (1932): 3570–3582, https://doi.org/10.1021/ja01348a011.

46. H. O. Pritchard and H. A. Skinner, "The Concept of Electronegativity," *Chemical Reviews* 55 (1955): 745–786, https://doi.org/10.1021/cr50004a005.

47. L. Pauling, "The Origin and Nature of the Electronegativity Scale," *Journal of Chemical Education* 65 (1988): 375, https://doi.org/10.1021/ed065p375.1.

48. H. Tandon, M. Labarca, and T. Chakraborty, "A Scale of Atomic Electronegativity Based on Floating Spherical Gaussian Orbital Approach," *ChemistrySelect* 6 (2021): 5622–5627, https://doi.org/10.1002/slct.202101142.

49. P. F. Lang, "Revisiting Electronegativity and Electronegativity Scales," *Journal of Chemical Education* 102 (2025): 424–429, https://doi.org/10.1021/acs.jchemed.4c01353.

50. J. Rumble, ed., *CRC Handbook of Chemistry and Physics*, 104th ed. (CRC Press), 2023–2024.

51. S. Chen, J. Ishii, S. Horiuchi, M. Yoshizawa-Fujita, and E. I. Izgorodina, "Difference in Chemical Bonding Between Lithium and Sodium Salts: Influence of Covalency on Their Solubility," *Physical Chemistry Chemical Physics* 19 (2017): 17366–17372, https://doi.org/10.1039/c7cp03009f.

52. Y. Zhao, Q. Liu, X. Zhao, et al., "Structure Evolution of Layered Transition Metal Oxide Cathode Materials for Na-Ion Batteries: Issues, Mechanism and Strategies," *Materials Today* 62 (2023): 271–295, https://doi.org/10.1016/j.mattod.2022.11.024.

53. C. Zhao, Q. Wang, Z. Yao, et al., "Rational Design of Layered Oxide Materials for Sodium-Ion Batteries," *Science* 370 (2020): 708–711, https://doi.org/10.1126/science.aay9972.

54. J. H. Yang, H. Kim, and G. Ceder, "Insights Into Layered Oxide Cathodes for Rechargeable Batteries," *Molecules* 26 (2021): 3173, https://doi.org/10.3390/molecules26113173.

55. K. Mizushima, P. C. Jones, P. J. Wiseman, and J. B. Goodenough, "Li_xCoO_2 (0<x<-1): A New Cathode Material for Batteries of High Energy Density," *Materials Research Bulletin* 15 (1980): 783–789, https://doi.org/10.1016/0025-5408(80)90012-4.

56. J. B. Goodenough, K. Mizushima, and P. J. Wiseman, Electrochemical Cell and Method of Making Ion Conductors for Said Cell (European Patent Office, EP 0017400 A1, 1980).

57. C. Xu, J. Zhao, C. Yang, and Y. S. Hu, "Polyanionic Cathode Materials for Practical Na-Ion Batteries Toward High Energy Density and Long Cycle Life," *ACS Central Science* 9 (2023): 1721–1736, https://doi.org/10.1021/acscentsci.3c00907.

58. W. Zhao, C. Zhao, H. Wu, L. Li, and C. Zhang, "Progress, Challenge and Perspective of Graphite-Based Anode Materials for Lithium Batteries: A Review," *Journal of Energy Storage* 81 (2024): 110409, https://doi.org/10.1016/j.est.2023.110409.

59. S. Chen, C. Liu, R. Feng, et al., "Natural Graphite Anode for Advanced Lithium-Ion Batteries: Challenges, Progress, and Perspectives," *Chemical Engineering Journal* 503 (2025): 158116, https://doi.org/10.1016/j.cej.2024.158116.

60. R. E. Franklin, "Crystallite Growth in Graphitizing and Non-Graphitizing Carbons," *The Royal Society* 209 (1951): 196–218, https://doi.org/10.1098/rspa.1951.0197.

61. P. J. F. Harris, "Structural Models of Non-Graphitising Carbon: A Brief History," *C* 11 (2025): 78, https://doi.org/10.3390/c11040078.

62. S. Qiu, L. Xiao, M. L. Sushko, et al., "Manipulating Adsorption–Insertion Mechanisms in Nanostructured Carbon Materials for High-Efficiency Sodium Ion Storage," *Advanced Energy Materials* 7 (2017): 1700403, https://doi.org/10.1002/aenm.201700403.

63. X. Dou, I. Hasa, D. Saurel, et al., "Hard Carbons for Sodium-Ion Batteries: Structure, Analysis, Sustainability, and Electrochemistry," *Materials Today* 23 (2019): 87–104, https://doi.org/10.1016/j.mattod.2018.12.040.

64. N. LeGe, X.-X. He, Y.-X. Wang, et al., "Reappraisal of Hard Carbon Anodes for Practical Lithium/Sodium-Ion Batteries From the Perspective of Full-Cell Matters," *Energy & Environmental Science* 16 (2023): 5688–5720, https://doi.org/10.1039/d3ee02202a.

65. Y. Li, A. Vasileiadis, Q. Zhou, et al., "Origin of Fast Charging in Hard Carbon Anodes," *Nature Energy* 9 (2024): 134–142, https://doi.org/10.1038/s41560-023-01414-5.

66. J. Yin and W. Zhang, "First-Principles Calculation of Electronic Structure and Optical Properties of F-Doped Diamond," *Journal of Electronic Materials* 160 (2025): 112983, https://doi.org/10.1016/j.diamond.2025.112983.

67. X. Chen, Y. Fang, J. Tian, et al., "Electrochemical Insight Into the Sodium-Ion Storage Mechanism on a Hard Carbon Anode," *ACS Applied Materials & Interfaces* 13 (2021): 18914–18922, https://doi.org/10.1021/acsami.1c03748.

68. D. Cheng, X. Zhou, H. Hu, et al., "Electrochemical Storage Mechanism of Sodium in Carbon Materials: A Study From Soft Carbon to Hard Carbon," *Carbon* 182 (2021): 758–769, https://doi.org/10.1016/j.carbon.2021.06.066.

69. L. Lyu, Y. Yi, and Z. L. Xu, "Graphite Co-Intercalation Chemistry in Sodium-Ion Batteries," *Batteries & Supercaps* 8 (2024): 202400521, https://doi.org/10.1002/batt.202400521.

70. Z. Wang, H. Yang, Y. Liu, et al., "Analysis of the Stable Interphase Responsible for the Excellent Electrochemical Performance of Graphite Electrodes in Sodium-Ion Batteries," *Small* 16, no. 51 (2020): 2003268, https://doi.org/10.1002/smll.202003268.

71. M. Goktas, C. Bolli, E. J. Berg, et al., "Graphite as Cointercalation Electrode for Sodium-Ion Batteries: Electrode Dynamics and the Missing Solid Electrolyte Interphase (SEI)," *Advanced Energy Materials* 8 (2018): 1702724, https://doi.org/10.1002/aenm.201702724.

72. X.-R. Zhang, J.-Y. Yang, Z.-Y. Ren, et al., "In-Situ Observation of Electrolyte-Dependent Interfacial Change of the Graphite Anode in Sodium-Ion Batteries by Atomic Force Microscopy," *New Carbon Materials* 37 (2022): 371–379, https://doi.org/10.1016/s1872-5805(22)60601-2.

73. S. S. Behara, J. Thomas, and A. Van der Ven, "Fundamental Thermodynamic, Kinetic, and Mechanical Properties of Lithium and Its Alloys," *Chemistry of Materials* 36 (2024): 7370–7387, https://doi.org/10.1021/acs.chemmater.4c01279.

74. C.-Y. Chou, M. Lee, and G. S. Hwang, "A Comparative First-Principles Study on Sodiation of Silicon, Germanium, and Tin for Sodium-Ion Batteries," *The Journal of Physical Chemistry C* 119 (2015): 14843–14850, https://doi.org/10.1021/acs.jpcc.5b01099.

75. W. P. Kalisvaart, B. C. Olsen, E. J. Luber, and J. M. Buriak, "Sb–Si Alloys and Multilayers for Sodium-Ion Battery Anodes," *ACS Applied Energy Materials* 2 (2019): 2205–2213, https://doi.org/10.1021/acsaem.8b02231.

76. A. J. Bard, R. Parsons, and J. Joedan, *Standard Potentials in Aqueous Solutions, International Union of Pure and Applied Chemistry* (Marcel Dekker, 1985).

77. M. Yamada, T. Watanabe, T. Gunji, J. Wu, and F. Matsumoto, "Review of the Design of Current Collectors for Improving the Battery Performance in Lithium-Ion and Post-Lithium-Ion Batteries," *Electrochem* 1 (2020): 124–159, https://doi.org/10.3390/electrochem1020011.

78. Q. Shi, C. Lu, Y. Cao, Y. Hao, A. Bachmatiuk, and M. H. Rümmeli, "Recent Developments in Current Collectors for Lithium Metal Anodes," *Materials Chemistry Frontiers* 7 (2023): 1298–1311, https://doi.org/10.1039/d3qm00029j.

79. T. Zheng and S. T. Boles, "Lithium Aluminum Alloy Anodes in Li-Ion Rechargeable Batteries: Past Developments, Recent Progress, and Future Prospects," *Progress Energy* 5 (2023): 032001, https://doi.org/10.1088/2516-1083/acd101.

80. P. Du, J. Wan, J. Qu, H. Xie, D. Wang, and H. Yin, "Passivation and Corrosion of Al Current Collectors in Lithium-Ion Batteries," *NPJ Materials Degradation* 8 (2024): 43, https://doi.org/10.1038/s41529-024-00453-x.

81. P. Adelhelm, P. Hartmann, C. L. Bender, M. Busche, C. Eufinger, and J. Janek, "From Lithium to Sodium: Cell Chemistry of Room Temperature Sodium–Air and Sodium–Sulfur Batteries," *Beilstein Journal of Nanotechnology* 6 (2015): 1016–1055, https://doi.org/10.3762/bjnano.6.105.

82. A. Rudola, C. J. Wright, and J. Barker, "Reviewing the Safe Shipping of Lithium-Ion and Sodium-Ion Cells: A Materials Chemistry Perspective," *Energy Material Advances* 2021 (2021): 9798460, https://doi.org/10.34133/2021/9798460.

83. X. Chen, X. Q. Zhang, H. R. Li, and Q. Zhang, "Cation−Solvent, Cation−Anion, and Solvent−Solvent Interactions With Electrolyte Solvation in Lithium Batteries," *Batteries & Supercaps* 2 (2019): 128–131, https://doi.org/10.1002/batt.201800118.

84. C. Reichardt and T. Welton, *Solvents and Solvent Effects in Organic Chemistry* (John Wiley & Sons, 2011).

85. Q. Liu, G. Tan, F. Wu, D. Mu, and B. Wu, "DFT Study of Solvation of Li^+/Na^+ in Fluoroethylene Carbonate/Vinylene Carbonate/Ethylene Sulfite Solvents for Lithium/Sodium-Based Battery," *Chinese Physics B* 30 (2021): 038203, https://doi.org/10.1088/1674-1056/abd763.

86. Y. Ugata, K. Shigenobu, R. Tatara, K. Ueno, M. Watanabe, and K. Dokko, "Solvate Electrolytes for Li and Na Batteries: Structures, Transport Properties, and Electrochemistry," *Physical Chemistry Chemical Physics* 23 (2021): 21419–21436, https://doi.org/10.1039/d1cp02946k.

87. K. Xu, "Nonaqueous Liquid Electrolytes for Lithium-Based Rechargeable Batteries," *Chemical Reviews* 104 (2004): 4303–4418, https://doi.org/10.1021/cr030203g.

88. V. Gutmann, "Coordination Chemistry of Certain Transition-Metal Ions. The Role of the Solvent," *Coordination Chemistry Reviews* 2 (1967): 239–256, https://doi.org/10.1016/s0010-8545(00)80206-4.

89. V. Gutmann, *Coordination Chemistry in Non-Aqueous Solutions* (Springer-Verlag, 1968).

90. K. J. Msayib and C. I. F. Watt, "Ion Pairing and Reactivity of Alkali Metal Alkoxides," *Chemical Society Reviews* 21 (1992): 237, https://doi.org/10.1039/cs9922100237.

91. J. Barthel, J. C. Justice, and R. Wachter, "Untersuchung der Elektrischen Leitfähigkeit Alkoholischer Alkalialkoholatlösungen," *Zeitschrift für Physikalische Chemie* 84 (1973): 100–113, https://doi.org/10.1524/zpch.1973.84.1-4.100.

92. A. F. Danil de Namor, E. E. Castellano, L. E. Pulcha Salazar, O. E. Piro, and O. Jafou, "Thermodynamics of Cation (Alkali-Metal) Complexation by 5,11,17,23-Tetra-Tert-Butyl[25,26,27,28-Tetrakis(2-Pyridylmethyl)oxy]-Calix(4)Arene and the Crystal Structure–Superstructure of its 1:1 Complex With Sodium and Acetonitrile," *Physical Chemistry Chemical Physics* 1 (1999): 285–293, https://doi.org/10.1039/a806902f.

93. A. F. D. de Namor, E. Gil, M. A. L. Tanco, et al., "Thermodynamics of Calix(4)Arene Esters. 1. Complexation of Alkyl p-terí-Butylcalix(4)Arenetetraethanoates and Alkali-Metal Cations in Acetonitrile and in Benzonitril," *The Journal of Physical Chemistry* 99 (1995): 16776–16780, https://doi.org/10.1021/j100045a044.

94. T. Nabeshima, "Regulation of Ion Recognition by Utilizing Information at the Molecular Level," *Coordination Chemistry Reviews* 148 (1996): 151–169, https://doi.org/10.1016/0010-8545(95)01164-1.

95. A. F. Danil De Namor, R. M. Cleverley, and M. L. Zapata-Ormachea, "Thermodynamics of Calixarene Chemistry," *Chemical Reviews* 98 (1998): 2495–2526, https://doi.org/10.1021/cr970095w.

96. A. F. Danil de Namor, "Solution Thermodynamics of Pyridinocalix(4)Arenes and Monovalent Cations," *Coordination Chemistry Reviews* 190-192 (1999): 283–295, https://doi.org/10.1016/s0010-8545(99)00071-5.

97. T. A. Pham, K. E. Kweon, A. Samanta, V. Lordi, and J. E. Pask, "Solvation and Dynamics of Sodium and Potassium in Ethylene Carbonate From ab Initio Molecular Dynamics Simulations," *The Journal of Physical Chemistry C* 121 (2017): 21913–21920, https://doi.org/10.1021/acs.jpcc.7b06457.

98. Z. Song, Z. Xing, J. Yang, et al., "Electrolyte Chemistry Development for Sodium-Based Batteries: A Blueprint from Lithium or a Step Toward Originality?," *Angewandte Chemie International Edition* 64 (2025): 202424543, https://doi.org/10.1002/anie.202424543.

99. L. Zhou, Z. Cao, W. Wahyudi, et al., "Electrolyte Engineering Enables High Stability and Capacity Alloying Anodes for Sodium and Potassium Ion Batteries," *ACS Energy Letters* 5 (2020): 766–776, https://doi.org/10.1021/acsenergylett.0c00148.

100. L. Zhou, Z. Cao, J. Zhang, et al., "Engineering Sodium-Ion Solvation Structure to Stabilize Sodium Anodes: Universal Strategy for Fast-Charging and Safer Sodium-Ion Batteries," *Nano Letters* 20 (2020): 3247–3254, https://doi.org/10.1021/acs.nanolett.9b05355.

101. Z. Tian, Y. Zou, G. Liu, et al., "Electrolyte Solvation Structure Design for Sodium Ion Batteries," *Advanced Science* 9 (2022): 2201207, https://doi.org/10.1002/advs.202201207.

102. Y. Wang, Z. Cao, W. Wahyudi, et al., "Electrolyte-Mediated Misconception of Carbon-Based Electrode Performance and Beyond in Metal-Ion Batteries," *Advanced Energy Materials* 13 (2023): 2301354, https://doi.org/10.1002/aenm.202301354.

103. Q. Li, Z. Cao, H. Cheng, et al., "Electrolyte Boosting Microdumbbell-Structured Alloy/Metal Oxide Anode for Fast-Charging Sodium-Ion Batteries," *ACS Materials Letters* 4 (2022): 2469–2479, https://doi.org/10.1021/acsmaterialslett.2c00841.

104. J. Wang, P. Kumar, Z. Ma, et al., "Electron-Donating or -Withdrawing Groups of Carbonate Solvent on Lithium-Ion (De)intercalation Chemistry," *ACS Energy Letters* 9 (2024): 4386–4398, https://doi.org/10.1021/acsenergylett.4c01920.

105. W. Niu, P.-T. Guo, M.-Y. Shen, et al., "High-Entropy-Driven Solvation Engineering for Sodium Ion Full Cell," *ACS Energy Letters* 10 (2025): 5542–5549, https://doi.org/10.1021/acsenergylett.5c02840.

106. L. Zheng, H. Zhang, P. Cheng, et al., "Li[$(FSO_2)(n\text{-}C_4F_9SO_2)N$] Versus $LiPF_6$ for Graphite/$LiCoO_2$ Lithium-Ion Cells at Both Room and Elevated Temperatures: A Comprehensive Understanding With Chemical, Electrochemical and XPS Analysis," *Electrochimica Acta* 196 (2016): 169–188, https://doi.org/10.1016/j.electacta.2016.02.152.

107. Z. Song, L. Zheng, P. Cheng, et al., "Taming the Chemical Instability of Lithium Hexafluorophosphate-Based Electrolyte With Lithium Fluorosulfonimide Salts," *Journal of Power Sources* 526 (2022): 231105, https://doi.org/10.1016/j.jpowsour.2022.231105.

108. M. Salomon, "Conductance of Solutions of Lithium Bis(Trifluoromethanesulfone)Imide in Water, Propylene Carbonate, Acetonitrile and Methyl Formate at 25°C," *Journal of Solution Chemistry* 22 (1993): 715–725, https://doi.org/10.1007/bf00647411.

109. P. Zhou, X. Zhang, Y. Xiang, and K. Liu, "Strategies to Enhance Li^+ Transference Number in Liquid Electrolytes for Better Lithium Batteries," *Nano Research* 16 (2022): 8055–8071, https://doi.org/10.1007/s12274-022-4833-1.

110. M. Ue, "Mobility and Ionic Association of Lithium and Quaternary Ammonium Salts in Propylene Carbonate and γ-Butyrolactone," *Journal of The Electrochemical Society* 141 (1994): 3336–3342, https://doi.org/10.1149/1.2059336.

111. S. Zugmann, M. Fleischmann, M. Amereller, R. M. Gschwind, H. D. Wiemhöfer, and H. J. Gores, "Measurement of Transference Numbers for Lithium Ion Electrolytes via Four Different Methods, a Comparative Study," *Electrochimica Acta* 56 (2011): 3926–3933, https://doi.org/10.1016/j.electacta.2011.02.025.

112. C. Wang, Z. Sun, Y. Liu, et al., "A Weakly Coordinating-Intervention Strategy for Modulating Na^+ Solvation Sheathes and Constructing Robust Interphase in Sodium-Metal Batteries," *Nature Communications* 15 (2024): 6292, https://doi.org/10.1038/s41467-024-50751-w.

113. D. Morales, L. G. Chagas, D. Paterno, S. Greenbaum, S. Passerini, and S. Suarez, "Transport Studies of $NaPF_6$ Carbonate Solvents-Based Sodium Ion Electrolytes," *Electrochimica Acta* 377 (2021): 138062, https://doi.org/10.1016/j.electacta.2021.138062.

114. Y. Okamoto, S. Tsuzuki, R. Tatara, K. Ueno, K. Dokko, and M. Watanabe, "High Transference Number of Na Ion in Liquid-State Sulfolane Solvates of Sodium Bis(Fluorosulfonyl)Amide," *The Journal of Physical Chemistry C* 124 (2020): 4459–4469, https://doi.org/10.1021/acs.jpcc.9b11458.

115. X. Zhou, Y. Huang, B. Wen, et al., "Regulation of Anion–Na^+ Coordination Chemistry in Electrolyte Solvates for Low-Temperature Sodium-Ion Batteries," *PNAS* 121 (2024): 2316914121, https://doi.org/10.1073/pnas.2316914121.

116. K. Xu, "Interfaces and Interphases in Batteries," *Journal of Power Sources* 559 (2023): 232652, https://doi.org/10.1016/j.jpowsour.2023.232652.

117. J. R. Fitzpatrick, B. E. Murdock, P. K. Thakur, et al., "An in-Depth Study of the Solid Electrolyte Interphase Compositional Evolution in Sodium-Ion Batteries: Unravelling the Effects of a Na Metal Counter Electrode on the SEI," *Advanced Science* 12 (2025): 04717, https://doi.org/10.1002/advs.202504717.

118. M. L. Holekevi Chandrappa, J. Qi, C. Chen, S. Banerjee, and S. P. Ong, "Thermodynamics and Kinetics of the Cathode–Electrolyte Interface in All-Solid-State Li–S Batteries," *Journal of the American Chemical Society* 144 (2022): 18009–18022, https://doi.org/10.1021/jacs.2c07482.

119. Y. Li, Y. Li, A. Pei, et al., "Atomic Structure of Sensitive Battery Materials and Interfaces Revealed by Cryo–Electron Microscopy," *Science* 358 (2017): 506–510, https://doi.org/10.1126/science.aam6014.

120. J. Zhang, S. Ma, J. Zhang, et al., "Critical Review on Cathode Electrolyte Interphase Towards Stabilization for Sodium-Ion Batteries," *Nano Energy* 128 (2024): 109814, https://doi.org/10.1016/j.nanoen.2024.109814.

121. Y. N. Wang, Y. Liu, X. Q. Zhang, et al., "In Situ Polymerized Polysiloxane Enables Cohesive Solid-Electrolyte Interphase for Practical Lithium-Metal Batteries," *Advanced Materials* 38 (2025): 19565, https://doi.org/10.1002/adma.202519565.

122. B. Jagger and M. Pasta, "Solid Electrolyte Interphases in Lithium Metal Batteries," *Joule* 7 (2023): 2228–2244, https://doi.org/10.1016/j.joule.2023.08.007.

123. E. Peled, "The Electrochemical Behavior of Alkali and Alkaline Earth Metals in Nonaqueous Battery Systems—The Solid Electrolyte Interphase Model," *Journal of The Electrochemical Society* 126 (1979): 2047–2051, https://doi.org/10.1149/1.2128859.

124. X. Cao, X. Ren, L. Zou, et al., "Monolithic Solid–Electrolyte Interphases Formed in Fluorinated Orthoformate-Based Electrolytes Minimize Li Depletion and Pulverization," *Nature Energy* 4 (2019): 796–805, https://doi.org/10.1038/s41560-019-0464-5.

125. H. Wu, H. Jia, C. Wang, J. G. Zhang, and W. Xu, "Recent Progress in Understanding Solid Electrolyte Interphase on Lithium Metal Anodes," *Advanced Energy Materials* 11 (2020): 2003092, https://doi.org/10.1002/aenm.202003092.

126. N. Pilling and R. Bedworth, "Magnesium Alloys in Biomedical Application," *Chemisches Zentralblatt* 94 (1923): 318–318.

127. G. G. Eshetu, G. A. Elia, M. Armand, et al., "Electrolytes and Interphases in Sodium-Based Rechargeable Batteries: Recent Advances and Perspectives," *Advanced Energy Materials* 10 (2020): 2000093, https://doi.org/10.1002/aenm.202000093.

128. K. Lim, J. Popovic, and J. Maier, "Ion Transport and Growth Behavior of Solid Electrolyte Interphases on Li and Na With Liquid Electrolytes Based on Impedance Analysis," *Journal of Materials Chemistry A* 11 (2023): 5725–5733, https://doi.org/10.1039/d2ta09189e.

129. Z. Ju, T. Zheng, B. Zhang, and G. Yu, "Interfacial Chemistry in Multivalent Aqueous Batteries: Fundamentals, Challenges, and Advances," *Chemical Society Reviews* 53 (2024): 8980–9028, https://doi.org/10.1039/d4cs00474d.

130. H. Kang, H. Kang, M. Lyu, and E. Cho, "A Review of Recent Developments in the Design of Electrolytes and Solid Electrolyte Interphase for Lithium Metal Batteries," *EcoMat* 6 (2024): 12498, https://doi.org/10.1002/eom2.12498.

131. S. Shi, P. Lu, Z. Liu, et al., "Direct Calculation of Li-Ion Transport in the Solid Electrolyte Interphase," *Journal of the American Chemical Society* 134 (2012): 15476–15487, https://doi.org/10.1021/ja305366r.

132. B. R. Das Goswami, V. Jabbari, R. Shahbazian-Yassar, F. Mashayek, and V. Yurkiv, "Unraveling ion Diffusion Pathways and Energetics in Polycrystalline Sei of Lithium-Based Batteries: Combined Cryo-HRTEM and DFT Study," *The Journal of Physical Chemistry C* 127 (2023): 21971–21979, https://doi.org/10.1021/acs.jpcc.3c05395.

133. K. Zhang, Y. Ji, Q. Wu, S. A. Nabavizadeh, Y. Qi, and L.-Q. Chen, "Simulating Solid Electrolyte Interphase Formation Spanning 10 8 Time Scales With an Atomically Informed Phase-Field Model," *Energy & Environmental Science* 18 (2025): 7541–7554, https://doi.org/10.1039/d5ee01030f.

134. J. Wagner-Henke, D. Kuai, M. Gerasimov, F. Roder, P. B. Balbuena, and U. Krewer, "Knowledge-Driven Design of Solid-Electrolyte Interphases on Lithium Metal via Multiscale Modelling," *Nature Communications* 14 (2023): 6823, https://doi.org/10.1038/s41467-023-42212-7.

135. X.-X. Ma, X. Shen, X. Chen, et al., "The Origin of Fast Lithium-Ion Transport in the Inorganic Solid Electrolyte Interphase on Lithium Metal Anodes," *Small Structures* 3 (2022): 2200071, https://doi.org/10.1002/sstr.202200071.

136. J. Pan, Y.-T. Cheng, and Y. Qi, "General Method to Predict Voltage-Dependent Ionic Conduction in a Solid Electrolyte Coating on Electrodes," *Physical Review B* 91 (2015): 134116, https://doi.org/10.1103/PhysRevB.91.134116.

137. Q. Zhang, J. Pan, P. Lu, et al., "Synergetic Effects of Inorganic Components in Solid Electrolyte Interphase on High Cycle Efficiency of Lithium Ion Batteries," *Nano Letters* 16 (2016): 2011–2016, https://doi.org/10.1021/acs.nanolett.5b05283.

138. N. Wang, Y. Xu, J. R. Horsley, et al., "Ultrafast Knock-Off Li^+ Diffusion and Subtle Structural Evolution of $Li_5V_3O_8$ Anode in Lithium-Ion Batteries," *ACS Nano* 18 (2024): 20123–20132, https://doi.org/10.1021/acsnano.4c02036.

139. X. Zhou, Q. Zhang, Z. Zhu, Y. Cai, H. Li, and F. Li, "Anion-Reinforced Solvation for a Gradient Inorganic-Rich Interphase Enables High-Rate and Stable Sodium Batteries," *Angewandte Chemie* 61 (2022): 202205045, https://doi.org/10.1002/anie.202205045.

140. L. Köbbing, A. Latz, and B. Horstmann, "Growth of the Solid-Electrolyte Interphase: Electron Diffusion Versus Solvent Diffusion," *Journal of Power Sources* 561 (2023): 232651, https://doi.org/10.1016/j.jpowsour.2023.232651.

141. A. Gajan, K. Var, R. Rajendiran, et al., "Dynamics of Transition Metal Dissolution and Cross-Contamination in Operating Lithium-Ion Batteries," *Journal of Power Sources* 630 (2025): 236031, https://doi.org/10.1016/j.jpowsour.2024.236031.

142. C. Delacourt, A. Kwong, X. Liu, et al., "Effect of Manganese Contamination on the Solid-Electrolyte-Interphase Properties in Li-Ion Batteries," *Journal of The Electrochemical Society* 160 (2013): A1099–A1107, https://doi.org/10.1149/2.035308jes.

143. S. R. Gowda, K. G. Gallagher, J. R. Croy, M. Bettge, M. M. Thackeray, and M. Balasubramanian, "Oxidation State of Cross-Over Manganese Species on the Graphite Electrode of Lithium-Ion Cells," *Physical Chemistry Chemical Physics* 16 (2014): 6898, https://doi.org/10.1039/c4cp00764f.

144. J. Xiao, N. Adelstein, Y. Bi, et al., "Assessing Cathode–Electrolyte Interphases in Batteries," *Nature Energy* 9 (2024): 1463–1473, https://doi.org/10.1038/s41560-024-01639-y.

145. S. Jo, S. Seo, S. K. Kang, et al., "Thermal Runaway Mechanism in Ni-Rich Cathode Full Cells of Lithium-Ion Batteries: The Role of Multidirectional Crosstalk," *Advanced Materials* 36 (2024): 2402024, https://doi.org/10.1002/adma.202402024.

146. R. Mogensen, D. Brandell, and R. Younesi, "Solubility of the Solid Electrolyte Interphase (SEI) in Sodium ion Batteries," *ACS Energy Letters* 1 (2016): 1173–1178, https://doi.org/10.1021/acsenergylett.6b00491.

147. L. A. Ma, A. J. Naylor, L. Nyholm, and R. Younesi, "Strategies for Mitigating Dissolution of Solid Electrolyte Interphases in Sodium-Ion Batteries," *Angewandte Chemie International Edition* 60 (2021): 4855–4863, https://doi.org/10.1002/anie.202013803.

148. G. G. Eshetu, H. Zhang, X. Judez, et al., "Production of High-Energy Li-Ion Batteries Comprising Silicon-Containing Anodes and Insertion-Type Cathodes," *Nature Communications* 12 (2021): 5459, https://doi.org/10.1038/s41467-021-25334-8.

149. J. Asenbauer, T. Eisenmann, M. Kuenzel, A. Kazzazi, Z. Chen, and D. Bresser, "The Success Story of Graphite as a Lithium-Ion Anode Material–Fundamentals, Remaining Challenges, and Recent Developments Including Silicon (Oxide) Composites," *Sustainable Energy Fuels* 4 (2020): 5387–5416, https://doi.org/10.1039/d0se00175a.

150. Y. Du, Y. Qiu, R. Zhuang, et al., "Superior Initial Coulombic Efficiency and Areal Capacity of Hard Carbon Anode Enabled by Graphite-Assisted Carbonization for Sodium-Ion Battery," *Carbon* 221 (2024): 118929, https://doi.org/10.1016/j.carbon.2024.118929.

151. R. Tian, S. H. Park, P. J. King, et al., "Quantifying the Factors Limiting Rate Performance in Battery Electrodes," *Nature Communications* 10 (2019): 1933, https://doi.org/10.1038/s41467-019-09792-9.

152. B. Lee, E. Paek, D. Mitlin, and S. W. Lee, "Sodium Metal Anodes: Emerging Solutions to Dendrite Growth," *Chemical Reviews* 119 (2019): 5416–5460, https://doi.org/10.1021/acs.chemrev.8b00642.

153. G. Li, X. Lou, C. Peng, C. Liu, and W. Chen, "Interface Chemistry for Sodium Metal Anodes/Batteries: A Review," *Chemical Synthesis* 2 (2022): 16, 10.20517/cs.2022.19.

154. N. G. Ningappa, K. Vishweswariah, M. D. Bouguern, A. K. M. R, K. Amine, and K. Zaghib, "Mechanistic Insights and Materials Strategies for Dendrite-Free Metal Anodes in Alkali and Zinc Batteries," *Nano Energy* 141 (2025): 111144, https://doi.org/10.1016/j.nanoen.2025.111144.

155. Y. Liu, R. Zhang, J. Wang, and Y. Wang, "Current and Future Lithium-Ion Battery Manufacturing," *iScience* 24 (2021): 102332, https://doi.org/10.1016/j.isci.2021.102332.

156. F. Schomburg, B. Heidrich, S. Wennemar, et al., "Lithium-Ion Battery Cell Formation: Status and Future Directions Towards a Knowledge-Based Process Design," *Energy & Environmental Science* 17 (2024): 2686–2733, https://doi.org/10.1039/d3ee03559j.

157. L. Streck, T. Roth, H. Bosch, et al., "Self-Discharge and Calendar Aging Behavior of Li-Ion and Na-Ion Cells," *Journal of The Elec-*

trochemical Society 171 (2024): 080531, https://doi.org/10.1149/1945-7111/ad6cfd.

158. L. Lu, X. Han, J. Li, J. Hua, and M. Ouyang, "A Review on the Key Issues for Lithium-Ion Battery Management in Electric Vehicles," *Journal of Power Sources* 226 (2013): 272–288, https://doi.org/10.1016/j.jpowsour.2012.10.060.

159. W. M. Seong, K.-Y. Park, M. H. Lee, et al., "Abnormal Self-Discharge in Lithium-Ion Batteries," *Energy & Environmental Science* 11 (2018): 970–978, https://doi.org/10.1039/c8ee00186c.

160. T. Roth, L. Streck, A. Graule, P. Niehoff, and A. Jossen, "Relaxation Effects in Self-Discharge Measurements of Lithium-Ion Batteries," *Journal of The Electrochemical Society* 170 (2023): 020502, https://doi.org/10.1149/1945-7111/acb669.

161. B. Babu, "Self-Discharge in Rechargeable Electrochemical Energy Storage Devices," *Energy Storage Mater* 67 (2024): 103261, https://doi.org/10.1016/j.ensm.2024.103261.

162. X. Pu, Y. Zheng, A. Qi, et al., "Understanding and Illustrating the Irreversible Self-Discharge in Rechargeable Batteries by the Evans Diagram," *Carbon Neutralization* 3 (2024): 94–107, https://doi.org/10.1002/cnl2.106.

163. P. Phogat, S. Dey, and M. Wan, "Powering the Sustainable Future: A Review of Emerging Battery Technologies and Their Environmental Impact," *RSC Sustainability* 3 (2025): 3266–3306, https://doi.org/10.1039/d5su00127g.

164. J. Zhao, L. Zhao, K. Chihara, et al., "Electrochemical and Thermal Properties of Hard Carbon-Type Anodes for Na-Ion Batteries," *Journal of Power Sources* 244 (2013): 752–757, https://doi.org/10.1016/j.jpowsour.2013.06.109.

165. G. G. Eshetu, S. Grugeon, H. Kim, et al., "Comprehensive Insights Into the Reactivity of Electrolytes Based on Sodium Ions," *ChemSusChem* 9 (2016): 462–471, https://doi.org/10.1002/cssc.201501605.

166. J. B. Robinson, D. P. Finegan, T. M. M. Heenan, et al., "Microstructural Analysis of the Effects of Thermal Runaway on Li-Ion and Na-Ion Battery Electrodes," *Journal of Electrochemical Energy Conversion and Storage* 15 (2018): 011010, https://doi.org/10.1115/1.4038518.

167. B. S. Vishnugopi, A. Sengupta, D. R. R. Kannan, et al., "Perspective on Thermal Stability and Safety of Sodium-Ion Batteries," *ACS Energy Letters* 10 (2025): 5383–5397, https://doi.org/10.1021/acsenergylett.5c02345.

168. Q. Li, Y. Li, M. Liu, et al., "Elucidating Thermal Decomposition Kinetic Mechanism of Charged Layered Oxide Cathode for Sodium-Ion Batteries," *Advanced Materials* 37 (2025): 2415610, https://doi.org/10.1002/adma.202415610.

169. W. Zuo, J. Qiu, X. Liu, et al., "The Stability of P2-Layered Sodium Transition Metal Oxides in Ambient Atmospheres," *Nature Communications* 11 (2020): 3544, https://doi.org/10.1038/s41467-020-17290-6.

170. Z. Cui and A. Manthiram, "Thermal Stability and Outgassing Behaviors of High-Nickel Cathodes in Lithium-Ion Batteries," *Angewandte Chemie International Edition* 62 (2023): 202307243, https://doi.org/10.1002/anie.202307243.

171. C. Heubner, M. Schneider, and A. Michaelis, "Heat Generation Rates of $NaFePO_4$ Electrodes for Sodium-Ion Batteries and $LiFePO_4$ Electrodes for Lithium-Ion Batteries: A Comparative Study," *Journal of Solid State Electrochemistry* 22 (2017): 1099–1108, https://doi.org/10.1007/s10008-017-3828-4.

172. Y.-Y. Wang, Y.-L. Xu, and R.-T. Guo, "A Review on the Thermal Stability of Sodium-Ion Battery Cathode Materials," *Journal of Energy Storage* 141 (2026): 119473, https://doi.org/10.1016/j.est.2025.119473.

173. M. Flugel, T. Waldmann, M. Kasper, and M. Wohlfahrt-Mehrens, "Detection of Copper Deposition on Anodes of Over-Discharged Lithium Ion Cells by GD-OES Depth Profiling," *ChemPhysChem* 21 (2020): 2047–2050, https://doi.org/10.1002/cphc.202000333.

174. G. G. Eshetu, J.-P. Bertrand, A. Lecocq, et al., "Fire Behavior of Carbonates-Based Electrolytes Used in Li-Ion Rechargeable Batteries With a Focus on the Role of the $LiPF_6$ and LiFSI Salts," *Journal of Power Sources* 269 (2014): 804–811, https://doi.org/10.1016/j.jpowsour.2014.07.065.

175. P. T. Bhutia, S. Grugeon, J.-P. Bertrand, et al., "Fire Hazards of Carbonate-Based Electrolytes for Sodium-Ion Batteries: What Changes From Lithium-Ion Batteries?," *Journal of Power Sources* 622 (2024): 235234, https://doi.org/10.1016/j.jpowsour.2024.235234.

176. H. Laufen, S. Klick, H. Ditler, et al., "Multi-Method Characterization of a Commercial 1.2 Ah Sodium-Ion Battery Cell Indicates Drop-in Potential," *Cell Reports Physical Science* 5 (2024): 101945, https://doi.org/10.1016/j.xcrp.2024.101945.

Biographies

Xingxing Wang obtained her Ph.D. (2025) from Huazhong University of Science and Technology (HUST), supervised jointly by Prof. Zhibin Zhou and Prof. Heng Zhang. Her research activities mainly focused on the design of non-aqueous electrolytes and the conversion mechanism of carbon fluoride battery. Following the completion of her doctoral studies, she joined Prof. Heng ZHANG's research group as a postdoctoral researcher — continuing to specialize in the development and fundamental investigation of non-aqueous electrolytes for rechargeable batteries.

Ziyu Song received his Ph.D. degree in Chemistry from HUST under the supervision of Prof. Heng Zhang. His research activities are mainly focused on the solvation behavior in organic electrolytes and ion transport at the interface/interphases between electrolyte and alkali metal electrodes. In 2025, he joined CIC EnergiGUNE as a Researcher working with Prof. Michel Armand. Currently, he concentrates on the visualization of the electrocrystallization of alkali metals in rechargeable batteries.

Wenfang Feng obtained her Ph.D. (2009) from Tongji Medical College at HUST. Then, she worked in Tongji Medical College and the School of Chemistry and Chemical Engineering at HUST. Presently, she is an Associated Professor of Organic Chemistry at HUST. Her research activities mainly resolve around ionic liquids and safe electrolyte materials for rechargeable batteries.

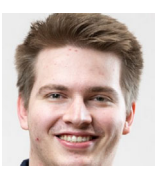

Moritz Schütte, M.Sc., works as a Research Associate and Ph.D. student at the Chair for Electrochemical Energy Conversion and Storage Systems (ISEA) of Prof. Dr. Dirk Uwe Sauer, RWTH Aachen University, with a Master's degree specializing in Process and Energy Engineering. He worked during his Bachelor's and Master's theses and as a student assistant at ISEA, focusing on aging analysis under thermal gradients and physico-chemical modeling of sodium-ion batteries. As a Ph.D. student in the department of battery modeling, analytics, and lifetime prediction, Schütte's research targets sodium-ion batteries, physico-chemical modeling, aging in commercial cells, and electrolyte development for enhanced performance and stability.

Sascha Berg received his Master's Degree in Electrical Engineering from RWTH Aachen University, Germany, in 2020. In 2020, he also joined the Chair for Ageing and Lifetime Prediction of Batteries of Prof. Dr. Egbert Figgemeier (ISEA, RWTH Aachen University, Germany) as a Ph.D. student. Since 2024, he works at Helmholtz Institute Münster, Forschungszentrum Jülich (Section Aachen), Münster, Germany in the group of Prof. Dr. Egbert Figgemeier. His research focuses on the aging effects caused by mechanical expansion during the operation of lithium-ion batteries and the optimization of

the tension in these batteries to minimize cyclic aging and improve performance. In addition, his research interests include investigating the mechanical and thermodynamic properties of the interphase that forms between lithium metal and liquid electrolyte.

Feng Cai obtained his M.Sc. degree in Sustainable Energy Supply in 2025 from RWTH Aachen University, Germany, under the supervision of Prof. Dr. Egbert Figgemeier and Prof. Dr. Dirk Uwe Sauer. His master's thesis focused on prelithiation of silicon-anode based lithium-ion batteries. He then joined the Institute for Power Electronics and Electrical Drives (ISEA) at RWTH Aachen University in the same research group and is currently pursuing his Ph.D.under the supervision of Prof. Dr. Egbert Figgemeier and Dr. Gebrekidan Gebresilassie Eshetu. His current research focuses on electrolyte development for aqueous sodium-ion batteries.

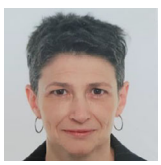

Viviane Maccio-Figgemeier earned her Ph.D. in Chemistry from Uppsala University, Sweden, in 2000. She subsequently completed a postdoctoral fellowship at the University of Basel from 2001 to 2003. From 2003 to 2006, she worked as a research scientist at Synphabase, a custom synthesis company. Since 2021, she has been employed as a research associate at the Helmholtz Institute Münster, Forschungszentrum Jülich (Section Aachen), in Münster, Germany. Her current research focuses on post-mortem and operando analysis of battery materials using Raman spectroscopy, with the aim of gaining deeper insight into the processes occurring during the charge and discharge of lithium- and sodium-based batteries.

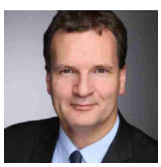

Dirk Uwe Sauer studied Physics at Technische Universität Darmstadt (1989–1994) and earned his Ph.D. in Electrochemistry from Universität Ulm in 2003 under Prof. Garche, with a thesis on optimizing lead-acid batteries in photovoltaic hybrid systems considering aging. Prior to joining RWTH Aachen as a Junior Professor in 2003 (promoted to associated professor in 2009 and full professor in 2012), he worked as a scientist, project leader, and head of group at Fraunhofer Institute for Solar Energy Systems ISE (1994–2003), focusing on energy storage, decentralized grid integration, and off-grid power supply. A key contributor to academia and industry, he co-founded four spin-off companies specializing in battery testing and BMS development, coordinated the BMBF Cluster of Excellence "Battery use concepts", and is a fellow of the National Academy of Science and Engineering (acatech), the Berlin-Brandenburg Academy of Sciences and Humanities, and The Academy of Sciences and Literature Mainz.

Stefano Passerini is Principal Scientist at the International Electrochemical Energy Storage Research Institute (IEES) and School of Energy and Mechanical Engineering at Nanjing Normal University, and Distinguished Senior Fellow at Karlsruhe Institute of Technology. His research focuses on the basic understanding and development of materials for high-energy batteries and supercapacitors, with the goal to create sustainable energy storage systems from environmentally friendly and available materials and processes. He has been awarded the Research Award of the Electrochemical Society Battery Division, and nominated Fellow of the International Society of Electrochemistry (2016) and the Electrochemical Society Inc (2020). Since 2019 he is a member of the Leopoldina German Academy of Science.

Michel Armand received his Ph.D. in Physics from Joseph Fourier University (1978). He has been the Directeur de Recherche at Centre National de la Recherche Scientifique (CNRS) since 1989 and Professor at the University of Montreal (1995–2004). He has ushered theoretical concepts leading to practical applications in energy-related electrochemistry. He has been one of the pioneers in the use of intercalation electrodes (1972), the introduction of the polymer electrolytes for battery application (1978), new salts based on delocalized anions of the sulfonimide family (1986), and organic electrode materials. He joined CIC EnergiGUNE as a Group Leader in solid electrolyte in 2013, and his present activities include new highly conductive polymers and techniques to obtain cross-linked networks, new highly delocalized negative charges, and new electrode materials.

Zhibin Zhou received his Ph.D. (2001) in Biomedical Engineering from HUST. He worked in the electrolyte conducting salts in the Mitsubishi chemical group, science and technology research center (2001–2003), and the National Institute of Advanced Industrial Science and Technology of Japan (2003–2006). He has been a Full Professor of Organic Chemistry at HUST since 2007. His research majorly focuses on developing fluorination methodologies for the preparation and commercialization of fluoroanions, especially fluorinated sulfonimide anions, for electrolyte materials of rechargeable batteries.

Egbert Figgemeier received his Ph.D. degree in chemistry from the University of Paderborn, Paderborn, Germany, in 1998. This was followed by academic research at University College Dublin, Dublin, Ireland, the University of Basel, Basel, Switzerland, and the University of Uppsala, Uppsala, Sweden. Since 2016, he has been the Group Leader with the Helmholtz Institute Münster, Forschungszentrum Jülich (Section Aachen), Münster, Germany. He also holds the Chair for "Ageing Processes and Lifetime Prediction of Batteries" at RWTH Aachen University, Aachen, Germany. His current research activities span from fundamental aging mechanisms in lithium-ion and lithium metal batteries to the development of designer electrolytes (salt anions and additives, prelithiation technologies, and interphase/interface studies).

Heng Zhang received his Ph.D. degree in Chemistry from HUST. Then, he joined CIC EnergiGUNE as a Post Doc Researcher (2016–2017) working with Prof. Michel Armand, and later he acted as the Research Line Manager of Polymer Electrolyte at CIC EnergiGUNE (January 2018–June 2020). Currently, he is a Full Professor of Organic Chemistry at HUST. Since 2024, he has been serving as a committee member of the International Symposium on Polymer Electrolytes (ISPE). His research interests mainly focus on the development of new fluorinated anions, ionic liquids, and alkali metal salts, and their nonaqueous electrolyte materials, particularly solid polymer electrolytes, aiming to providing industrially viable solutions in anion design for better rechargeable batteries.

Gebrekidan Gebresilassie Eshetu obtained his Ph.D. at the end of 2013 in Materials Science and Chemistry from the LRCS (Centre National de la Recherche Scientifique—CNRS) Laboratory in Amiens, France, under the supervision of Prof. Dr. Michel Armand, Prof. Dr. Stephane Laruele and Dr. Ing. Sylvie Grugeon. Following this, he did his postdoctoral research at the Karlsruhe Institute of Technology (KIT), Helmholtz Institute Ulm (HIU) in the group of Prof. Dr. Stefano Passerini. Then, he worked in CIC EnergiGUNE (Spain, 2016–2018) as a Senior Postdoctoral Researcher on solid electrolytes for rechargeable batteries. Subsequently, he joined RWTH Aachen University in the group of Prof. Dr. Egbert Figgemeier. Currently, he is a Group Leader of functional interfaces and interphases of electrochemical energy storage systems at RWTH Aachen University and holds an adjunct professorship of Materials Science and Engineering at Mekelle Institute of Technology of Mekelle University, Ethiopia. His research interest focuses on advanced electrolytes, modulating functional interfaces and interphases for rechargeable batteries.